



Department of Geology and Soil Science

Estimating flow patterns to an agricultural ditch by inverse modeling of temperature and salinity measurements

Pieter Winters

Academic year 2012–2013

*Internship report
1st Master of Science in Geology*

Supervisors: J. Delsman (Deltares)
G. Oude Essink (Deltares)
L. Lebbe (Ghent University)

Company: DELTARES

ACKNOWLEDGMENTS

Completing my internship learning experience and writing this paper would not have been possible without the support and help of several people. Hereby I thank Deltares for the admission to their facilities and its employees for their great hospitality. I would also like to thank Jasper Claus, Luc Lebbe, Gualbert Oude Essink and Alexander Vandenbohede for their helpful commentary. Finally, but foremost I thank Joost Delsman for his flawless guidance and assistance throughout the entire period of this internship.

Pieter Winters

LIST OF USED SYMBOLS

C^k = the concentration of species k [ML^{-3}]

c_{Pfluid} = the specific heat capacity of the fluid [$L^2T^{-2}\Theta^{-1}$]

c_{Psolid} = the specific heat capacity of the solid [$L^2T^{-2}\Theta^{-1}$]

C_s^k = the source or sink concentration of species k [ML^{-3}]

D_m^k = the molecular diffusion coefficient for species k [L^2T^{-1}]

h_0 = the hydraulic head measured in terms of the reference fluid of a specified concentration and temperature (commonly fresh water) [L]

K_0 = the hydraulic conductivity tensor of material saturated with the reference fluid [LT^{-1}]

K_d^k = the distribution coefficient of species k [L^3M^{-1}]

K_{Tbulk} = the bulk thermal conductivity of the aquifer material [$MLT^{-3}\Theta^{-1}$]

\bar{o} = the mean of the observed values

q'_s = a fluid source or sink with density ρ_s [T^{-1}]

\bar{s} = the mean of the simulated values

$S_{s,0}$ = the specific storage, defined as the volume of water released from storage per unit volume per unit decline of h_0 [L^{-1}]

T_s = source temperature [Θ]

μ_0 = dynamic viscosity of the reference fluid [$ML^{-1}T^{-1}$]

ρ_b = the bulk density [ML^{-3}]

ρ_s = the density of the solid [ML^{-3}]

μ = dynamic viscosity [$ML^{-1}T^{-1}$]

H_0 = the drawdown at time $t = 0$ [L]

H_t = the drawdown at time $t = t$ [L]

K = hydraulic conductivity [LT^{-1}]

L = a characteristic length [L]

L_e is the length of the screen [L]

LSQ = least square error

MV = mean value

n = number of days

NSC = Nash-Sutcliffe coefficient

o_t = observed value at day t

q = specific discharge [LT^{-1}]

R = the radius of the gravel envelope [L]

r_c = the radius of the well casing [L]

R_e = the effective radial distance over which head is dissipated [L]

s_t = simulated value at day t

t = day

T = temperature [Θ]

T = time since $H = H_0$ [T]

t = time [T]

z = elevation [L]

α = the dispersivity tensor [L]

θ is porosity [-]

ρ = the density of the fluid [ML^{-3}]

CONTENTS

Acknowledgments.....	II
List of Used Symbols	III
Contents.....	IV
1 Introduction.....	1
2 Theoretical background	2
2.1 Introduction to solute transport.....	2
2.2 Introduction to heat transport	3
2.3 Solute and heat transport analogy.....	5
3 Site description	7
4 Methods.....	8
4.1 Monitoring design.....	8
4.2 Field measurements	9
4.3 Numerical modeling	15
4.4 Model calibration.....	22
5 Results	22
5.1 Calibration	23
5.2 Distribution.....	26
6 Discussion.....	28
6.1 Groundwater- and solute transport towards ditch and drains	28
6.2 Interactions to precipitation	28
6.3 EC measurements	29
6.4 Utility of adding solute transport.....	30
6.5 Heat transport	30
7 Conclusion	31
8 References	32

1 INTRODUCTION

I have had the opportunity to do an internship at DELTARES, an independent institute for applied research in the field of water, subsurface and infrastructure (www.deltares.nl) based in the Netherlands. As a densely populated country, the Netherlands is faced with particular challenges having about 25 % of its surface below sea level. The Dutch coastal areas are characterized by upward seepage of saline and nutrient-rich groundwater into the deep polders. This leads to salinization of the surface water (DE LOUW, GRIFFIOEN & VAN DEN EERTWEGH, 2000; DE LOUW, OUDE ESSINK, STUYFZAND & VAN DER ZEE, 2010; OUDE ESSINK, 2001; VAN DEN EERTWEGH, NIEBER, DE LOUW, VAN HARDEVELD & BAKKUM, 2006; VAN PUIJENBROEK, JANSE & KNOOP, 2004; VAN REES VELLINGA, TOUSSAINT & WIT, 1981; WESSELING, 1980). Possible effects are salt damage to crops and unfit surface water for irrigation. The predicted climate change and associated sea level rise will only magnify these effects to coastal aquifers (OUDE ESSINK, 2001).

This internship study revolves around this burning issue. It is situated within the framework of “Project 2.1”, studying the interaction between groundwater and surface water under saline and dry conditions to find a climate-robust regional freshwater supply [DUTCH: interactie tussen grond- en oppervlaktewater onder zoute en droge omstandigheden voor het vinden van een klimaatrobuste regionale zoetwatervoorziening]. The main objective of Project 2.1 is to develop strategies for a robust freshwater supply in the future, through the development of a framework that can be used to evaluate the effects of measures on the groundwater/surface water system. This framework will be based on the knowledge of three important conditions:

1. System knowledge on the scale of a ditch
2. System knowledge on the scale of a polder
3. Modeling at different scales

For this work the focus is on the first condition, the system knowledge on the scale of a ditch. Recent research shows that sharp local gradients in salinity and temperature are indications for flux differences that occur on a scale of decimeters to meters (DE LOUW, OUDE ESSINK, GOES & SERGI, 2008; OUDE ESSINK, DE LOUW, STEVENS, DE VEEN, DE PREVO, MARCONI & GOES, 2009). Other studies show that the incorporation of solute and heat transport to groundwater modeling has many benefits (this will be explained in chapter 2). The primary goal of this internship was to make an inverse model that incorporates head,

concentration and temperature measurements, which can be used to estimate flow patterns to an agricultural ditch.

This paper seeks to describe all aspects covered during the internship. Chapter 2 addresses the overall background of the subject; hereby a summary is made of the literature study that was conducted as an introduction to this internship. This is followed by a clear description of the research area (chapter 3). Given that the emphasis of an internship is on learning and mastering new techniques and methods, the discussion of the methods (chapter 4) is described in great detail. The following facets are discussed: the monitoring design, the field measurements, the numerical modeling and the model calibration. After this, the results from the numerical model are summarized (chapter 5) and discussed (chapter 6).

2 THEORETICAL BACKGROUND

This section provides the outlines of solute and heat transport. First the backgrounds of both solute and heat transport are briefly stated, after which the analogy between solute and heat transport is discussed. For a more thorough impression see KONIKOW (2010) for solute transport and ANDERSON (2005) for heat transport. A more extensive and in-depth discussion can be found in GUO and LANGEVIN (2002) and LANGEVIN, THORNE, DAUSMAN, SUKOP and GUO (2007).

2.1 Introduction to solute transport

In comparison to head and flow modeling, it is far more complicated to model subsurface solute transport. One of the reasons is that the classical equation does not always effectively represent what is seen at field scale, thus the used numerical model solves the wrong equation. This is not inconceivable, because the mathematical properties of the transport equation vary depending on which terms in the equation are dominant. This manifests itself in the transport equation being hyperbolic where advection is dominant, and parabolic where hydrodynamic dispersion is dominant. No single numerical method can anticipate to this, thus no method is optimal in every situation (KONIKOW, 2010). Another reason for why the representation tends to fail, is that it is necessary to consider the groundwater flow equation and the equation of solute transport simultaneously in order to describe solute transport; this also contributes to the complexity.

Due to the complexity of modeling solute transport, one should try to keep the model itself as simple as possible. The development and application of the model consist of steps in an

evolutionary process: one should start simple and add increasing degrees of complexity so the effects of the added complexity (whether in processes, parameters, dimensionality, or boundary conditions) can be easily discerned. As stated by KONIKOW (2010): the secret to successful solute-transport modeling may simply be to lower expectations.

There are different field techniques, direct and indirect, that can be used to get information about solute transport (DE LOUW, EEMAN, SIEMON, VOORTMAN, GUNNINK, VAN BAAREN & OUDE ESSINK, 2011), examples are: groundwater sampling, TEC (temperature and electrical soil conductivity)-probe measurements, electrical cone penetration tests (ECPT), continuous vertical electrical soundings (CVES) and electromagnetic survey.

2.2 Introduction to heat transport

For more than 100 years researchers have used heat as a natural tracer for surface water and groundwater interaction (ONDERKA, BANZHAF, SCHEYTT & KREIN, 2013; SLICHTER, 1905). It is a naturally occurring tracer, free from institutional issues of contamination (CONSTANTZ, 2008). The fundamental concepts for the use of heat as a groundwater tracer were introduced in the 1960s, hereafter interest faded, although it never died out. Interest resurged in the late 1980s, with the publication of a methodology to use temperature profiles beneath streams to quantify the interaction between groundwater and streams (LAPHAM, 1989), together with a collection of papers describing the effects of groundwater flow on the thermal regime in basins (BECK, GARVEN & STEGENA, 1989). Recent work has greatly increased the amount of literature on heat as a tracer and temperature measurements as substitutes for head measurements, mainly in the field of temperature profile analysis to estimate interchange with streams (STONESTROM & CONSTANTZ, 2003). Additionally, several researchers have combined the use of flow and heat transport concepts to investigate deep and shallow groundwater systems (e.g. ANDREWS & ANDERSON, 1979; BAYER, GIRALDO, MENDEZ, RASUOLI, ZHENG & BLUM, 2008; BENSE & KOOI, 2004; BRAVO, JIANG & HUNT, 2002; BREDEHOEFT & PAPADOPOULOS, 1965; BUNDSCHUH, 1993; CONSTANTZ, THOMAS & ZELLWEGER, 1994; GRESKOWIAK, PROMMER, MASSMANN & NÜTZMANN, 2006; HATCH, FISHER, REVENAUGH, CONSTANTZ & RUEHL, 2006; JIANG & WOODBURY, 2006; KEERY, BINLEY, CROOK & SMITH, 2007; MARTIN, BENDER, GAULKE & WALLACE, 2001; PARSONS, 1970; PROMMER & STUYFZAND, 2005; RONAN, PRUDICK, THODAL & CONSTANTZ, 1998; SILLIMAN, RAMIREZ & MCCABE, 1995; TANIGUCHI, 1993; WOODBURY & SMITH, 1988; VANDENBOHEDE & LEBBE, 2010; ...).

There are two main reasons why there was a revived interest in subsurface temperatures for heat transport estimation (ANDERSON, 2005; MA & ZHENG, 2010). The first reason is the recent availability of improved temperature sensors and relatively inexpensive data loggers; with these tools it is possible to make remote and continuous measurements. Examples are: the application of thermocouples and thermistors to obtain a time series of measurements remotely (HATCH et al., 2006; KEERY et al., 2007), the application of fiber-optic distributed temperature sensors for providing high resolution lateral patterns (MUNZ, OSWALD & SCHMIDT, 2011; TYLER, SELKER, HUASNER, HATCH, TORGERSEN, THODAL & SCHLADOW, 2009) or the use of airborne thermal sensors to detect areas of groundwater discharge (BECKER, 2006). The second reason is the flourishing of improved numerical codes for simulating coupled groundwater flow and heat transport (ANDERSON, 2005). Some examples of these codes are: BASIN2, FEFLOW, MT3DMS, REACTRANS, SEAWAT, SHEMAT, SUTRA, TOUGH2, VS2DH (ANDERSON, 2005; LANGEVIN, THORNE, DAUSMAN, SUKOP & GUO, 2007, VANDENBOHEDE, LOUWYCK & LEBBE, 2008).

It is perhaps not surprising that temperature measurements are useful where there is a large contrast in surface water and groundwater temperatures (ANDERSON, 2005). On the other hand, if temperature measurements could only be used in those situations, the applications would be limited and useless for this study (where the interactions in the surficial zone are studied). Thankfully, SUZUKI (1960) and STALLMAN (1965) postulated that groundwater velocity could be estimated from seasonal fluctuations of temperature at the land surface. Using a version of Stallman's model, LAPHAM (1989) proved that monthly and yearly variations in subsurface temperature beneath streams can be used to estimate groundwater velocities. Similarly, BRAVO et al. (2002) used measurements of the surficial temperature in the parameter estimation process of a coupled groundwater and heat-flow model where the basal heat influx was relatively low (VANDENBOHEDE et al., 2008).

Since the availability of improved temperature sensors and numerical codes, investigators have started to explore the full potential of using temperature measurements in a wide variety of hydrogeological settings (ANDERSON, 2005). One of the most powerful applications of temperature data is in formal solutions for the inverse problem. Usually, the information obtained by measuring heads is insufficient to find unique values of inflows and parameters; for example, many combinations of hydraulic conductivity and recharge can give the same simulated head distribution (BRAVO et al., 2002). Adding information about the movement

of solute and/or heat can help constrain the calibration. This was proven in studies where field models that did not converge to an optimal parameter-set when only head data were used, did converge when head and temperature data were used (ANDERSON, 2005; BRAVO et al., 2002).

Finally it is important to remember that there are potential limitations to the use of subsurface temperatures (BRAVO et al., 2002). The head and temperature data have to be measured simultaneously and at a similar frequency in order to characterize the temporal nature of the water level and temperature fluctuations. It is also plausible that the stratigraphy that controls the groundwater flow (the hydro-stratigraphy) does not coincide with the stratigraphy that controls the thermal profiles, and thus the layering/geometry that best represents the flow system may not be the best representation for the heat transport system.

2.3 Solute and heat transport analogy

Analogue formulas of solute and heat transport highlight the similarities between the two processes. Based on these similarities the correct input values required by MT3DMS when representing heat transport are calculated. The following is a general form of the solute transport equation solved by MT3DMS (LANGEVIN et al., 2007; LANGEVIN, DAUSMAN & SUKOP, 2010):

$$\left(1 + \frac{\rho_b K_d^k}{\theta}\right) \frac{\partial(\theta C^k)}{\partial t} = \nabla \cdot \left[\theta \left(D_m^k + \alpha \frac{q}{\theta} \right) \cdot \nabla C^k \right] - \nabla \cdot (q C^k) - q'_s C_s^k \quad (1)$$

Next is a form of the heat transport equation, which was manipulated by THORNE, LANGEVIN and SUKOP (2006) to highlight the similarity with the solute transport equation (LANGEVIN et al., 2007; LANGEVIN et al., 2010):

$$\left(1 + \frac{1 - \theta}{\theta} \frac{\rho_s}{\rho} \frac{c_{Psolid}}{c_{Pfluid}}\right) \frac{\partial(\theta T)}{\partial t} = \nabla \cdot \left[\theta \left(\frac{K_{Tbulk}}{\theta \rho c_{Pfluid}} + \alpha \frac{q}{\theta} \right) \cdot \nabla T \right] - \nabla \cdot (q T) - q'_s T_s \quad (2)$$

Evaluation of Equations 1 and 2 reveals several important equivalences. The storage terms on the left sides of Equations 1 and 2 are prefixed with retardation terms. For solute transport, retardation is caused by adsorption of solutes through the aquifer matrix material. With heat transport, retardation is caused by heat transfer between the fluid and solid aquifer matrix (LANGEVIN et al., 2010). MT3DMS can be used to represent thermal retardation by calculating the distribution coefficient (K_d) for the temperature species as a function of thermal properties:

$$K_d^T = \frac{C_{Psolid}}{\rho c_{Pfluid}} \quad (3)$$

Inspection of Equations 1 and 2 also shows that heat conduction is mathematically equivalent to molecular solute diffusion. To represent heat conduction with MT3DMS, thermal diffusivity for the temperature species is calculated as follows:

$$D_m^T = \frac{K_{Tbulk}}{\theta \rho c_{Pfluid}} \quad (4)$$

The most remarkable difference between solute transport and heat transport is the difference between solute and thermal dispersivity. It is also important to mention here that there are conflicting ideas regarding the importance of thermal dispersion to heat (HATCH et al., 2006; LANGEVIN et al., 2010; VANDENBOHEDE et al., 2008). For solutes, mechanical dispersion frequently dominates molecular diffusion. This does not apply for heat transport because heat conduction is normally much stronger than thermal dispersion (ANDERSON, 2005; FERGUSON, 2007; LANGEVIN et al., 2010; VANDENBOHEDE et al., 2008; VANDENBOHEDE, HERMANS & NGUYEN, 2011). Therefore, thermal dispersion is often neglected (BEAR, 1972; HOPMANS, SIMUNEK & BRISTOW, 2002; INGEBRITSEN & SANFORD, 1998; WOODBURY & SMITH, 1985). Nevertheless other authors do not neglect the thermal dispersion. Some advocate the same order of magnitude for both thermal and solute dispersivity (DEMARSILY, 1986). Others report values for longitudinal and transverse thermal dispersivity equal to 100 m and 10 m (SMITH & CHAPMAN, 1983) or longitudinal thermal dispersivity values in the order of magnitude of 0.01 m to 1 m in case of water exchange between streams and groundwater reservoirs (NISWONGER & PRUDIC, 2003). CONSTANTZ, COX and SU (2003) derived that thermal dispersivity is significantly smaller than solute dispersivity. Regardless, the present formulation of the heat transport equation (Equation 2), solved by SEAWAT and MT3DMS, contains a thermal dispersion term, as this term is simply retained from the solute transport representation. A second difference between solute and heat dispersivity is that solute dispersivity increases with the scale of the test, while this effect is not so distinct with thermal dispersivity (GELHAR, WELTY & REHFELDT, 1992; VANDENBOHEDE & LEBBE, 2002; VANDENBOHEDE & LEBBE, 2003; VANDENBOHEDE & LEBBE, 2006; VANDENBOHEDE & LEBBE, 2008).

For heat transport where fluid density and viscosity variations are not expected to influence groundwater flow, the velocity distribution calculated by MODFLOW can be used with MT3DMS to simulate heat transport. This will be computationally more efficient (MA & ZHENG, 2010). But when the temperature variations are larger, density and viscosity effects may influence groundwater flow patterns. In these situations, where a greater accuracy is desired (MA & ZHENG, 2010), the SEAWAT program can be used to couple the flow and transport processes. SEAWAT solves the following form of the variable-density groundwater flow equation (LANGEVIN et al., 2007; LANGEVIN et al., 2010):

$$\nabla \cdot \left[\rho \frac{\mu_0}{\mu} K_0 \left(\nabla h_0 + \frac{\rho - \rho_0}{\rho_0} \nabla z \right) \right] = \rho S_{s,0} \frac{\partial h_0}{\partial t} + \theta \frac{\partial \rho}{\partial t} - \rho_s q'_s \quad (5)$$

This equation is based on a reference head (commonly a fresh water head) instead of pressure or a point water head. The fluid density and fluid viscosity are calculated using the appropriate equations (equation of state and equation for dynamic viscosity). For a better insight into this topic, see LANGEVIN et al. (2007).

3 SITE DESCRIPTION

This study is carried out in the Schermer polder, more precisely at one of the parcels of farmer Ted Vaalburg which is used to grow potatoes. This polder (latitude 52°35'58.30'', longitude 4°46'45.16'') is located in the village Schermer in the province of North Holland (see figure 1). The genesis of this polder lies in the draining of the Schermeer Lake. To the west of the polder there are beach plains and dunes, formed during the Holocene, to the east there are peat-polders.

The geology of the study-area is formed out of Holocene sediments; this package has a thickness of about 25 m. It consists primarily of marine clays alternated with less pervious sands (Westland Formation). This formation rests above Aeolian sands forming a confined aquifer. The upper part of this aquifer consists of the formation of Kreftenheije, the lower parts are the sands of the formation of Urk. Between these two formations a separation layer (Formation of Drente) is usually present, yet this formation is lacking in the Schermer polder (ACACIA WATER, 2013).

The deeper regional groundwater flow is west to east oriented. The groundwater flows from the coast to the deep polders, like the Schermer polder, where seepage water is discharged. This seepage water has a high chloride content and thus a salty character. Based on a regional

groundwater model it is approximated that the seepage to the Schermer polder is in the order of 0.50 – 0.75 mm/day (ACACIA WATER, 2011).

The parcel, with a length of 110 m, is a low lying area; the average ground level is around -4 m NAP (Nieuw Amsterdams Peil: the Dutch national ordinance level, approximately equal to mean sea level). One side of the field is bordered by a ditch. Perpendicular to the ditch there are tile drains located at a depth of 1.0 m Below Ground Level (BGL) with a horizontal spacing of 5 m. These drains have approximately the same length as the parcel (110 m). At the other side of the ditch a dike is situated with a road on the top. The elevation is 1.2 m higher than the parcel.

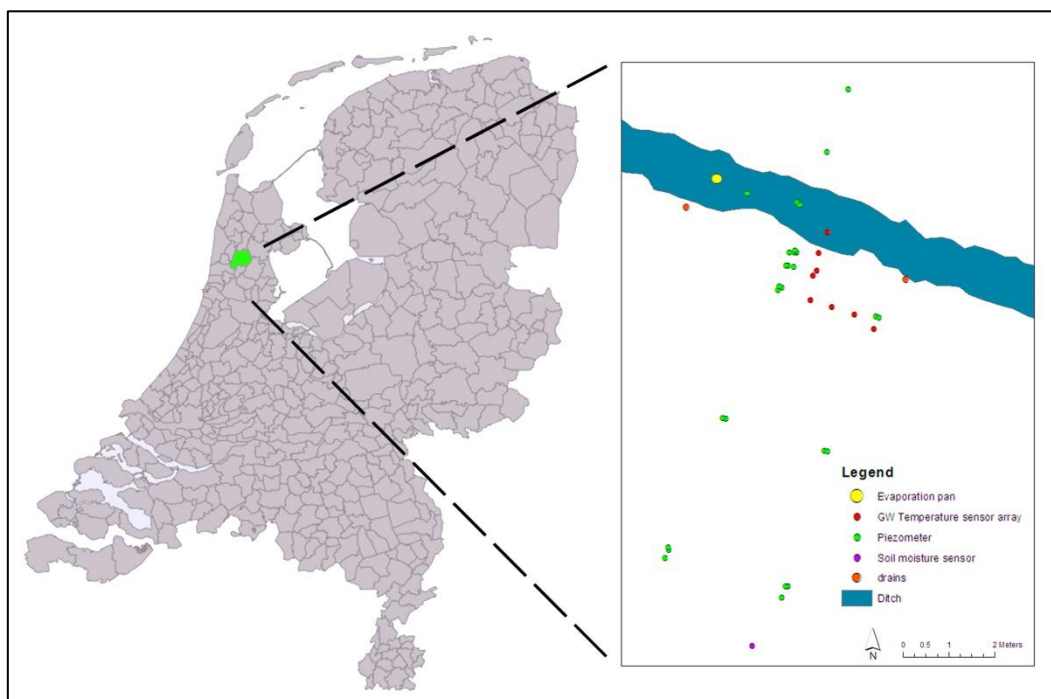


figure 1: Location of the study area, with an indication of the monitoring design (source: own research).

4 METHODS

4.1 Monitoring design

For Project 2.1, of which this study is a part, a comprehensive measurement setup was designed (see figure 1 and figure 2). Forty meters of the ditch is dammed by steel bulkheads to isolate it from the rest of the ditch. The water from the tile drains is kept isolated from the discharge directly into the ditch. The water from both the drains and the ditch is measured, by means of flow meters and EC-meters. Additionally the moisture conditions are measured with soil moisture sensors and monitoring wells (piezometer nests). In these piezometers the EC is

also measured. An array of temperature sensors is placed perpendicular to the ditch. Finally the surface water evaporation rate is measured with a floating evaporation pan, and a meteorological station measures the precipitation, temperature, wind and radiation. In the next chapter some techniques are explained more extensively with a thorough interpretation of the data.

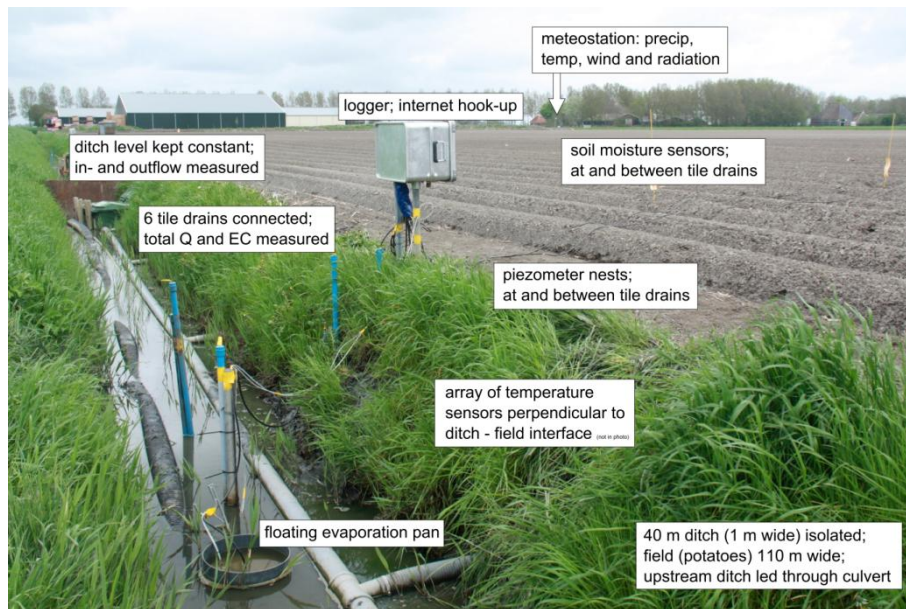


figure 2: Measurement design (source: personal communication, J. Delsman).

4.2 Field measurements

4.2.1 Precipitation and evaporation

During the period from 12 March 2012 until 31 December 2012 (290 days) meteorological data were obtained with a meteo-station and a floating evaporation pan. The precipitation was measured directly, while the evaporation was calculated with the Penman Monteith equation (for more information see MONTEITH, 1965). For this equation the air temperature, relative humidity, air pressure, incoming radiation (total and at top of atmosphere), day length, wind speed and elevation are used from the meteorological data. To improve the stability of the model it was opted to spread out precipitation peaks higher than 18 mm/day. Therefore all precipitation higher than 18 mm/day is moved to the next day. The result is shown in figure 3.

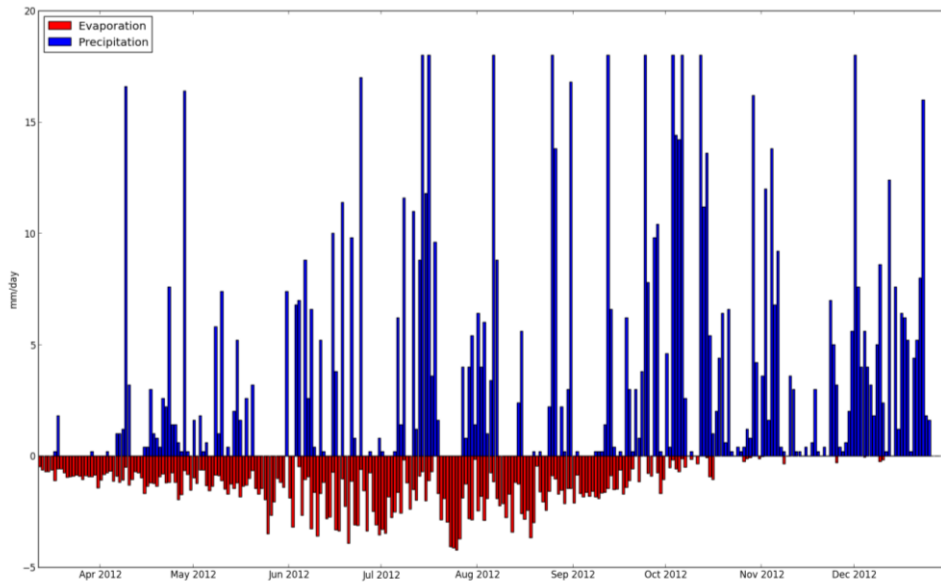


figure 3: Measured precipitation and calculated evaporation during the period of 12 March 2012 until 31 December 2012 (source: own research).

4.2.2 Investigation drilling

In this study the focus is on the upper zone of the subsurface which is called the surficial zone (PARSONS, 1970; VANDENBOHEDE & LEBBE, 2010). A total of 10 shallow drillings were made to a maximum depth of 2 m to get a clear insight of the underground; 6 of these drillings were made in an earlier study (ACACIA WATER, 2013) and 4 were made during this internship. These drillings show that the approximate thickness of the unsaturated zone is about 1 m, and composed of a clay layer in the first 30 to 50 cm on top of fine sand-loamy deposits with abundant marine shells. The fine sands occur until at least 17 m below surface, which corresponds to the bottom of a deeper drilling that was made in the vicinity (drilling B19D0247, DINOLOKET). These drillings also show that the soil structure knows no extreme variations within the parcel.

4.2.3 CVES

To get an insight of the depth and distribution of fresh water in the parcel, multiple 2D cross sections were made by means of Continuous Vertical Electrical Sounding (CVES). A CVES is made by inserting electrodes into the top soil in an array, and connecting them to a central device. This device, in this case the ABEM SAS4000 Terrameter, sends a current through different sets of electrodes while measuring the potential difference of the soil. Based on the profile length and the distance between different electrodes, the resolution and depth of the 2D cross section can be altered. Here a high resolution Schlumberger configuration was used (around 750 measurements per profile). Calculated with specific software (RES2Dinv from

GEOTOMO Software), an interpretation is made. From this interpretation the position and depth of fresh and brackish water can be deduced. Based on these measurements the transition of fresh to salt water is positioned around 2.0 to 3.5 m below the surface (ACACIA WATER, 2013). The position of the tile drains also appears with this method. These are located perpendicular to the ditch, are placed 5 m from each other and have a diameter of 60 mm. These drains are positioned 1.0 m below surface, into the fine sands. One CVES transect is shown in figure 4. The figure also shows the difference in drainage capacity between the old and the new tile drains. The new drains can drain more effectively; this translates to the brackish water being drawn more towards the new drains.

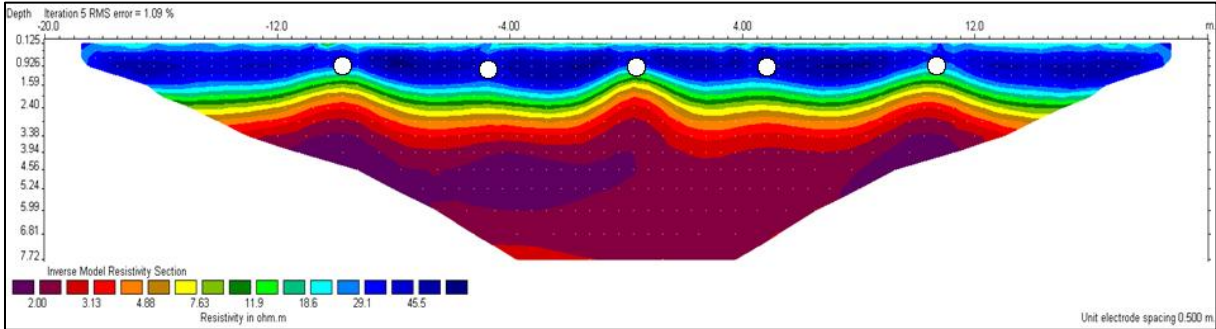


figure 4: CVES transect, parallel to the ditch (source: personal communication, J. Delsman).

4.2.4 Groundwater heads and EC-measurements

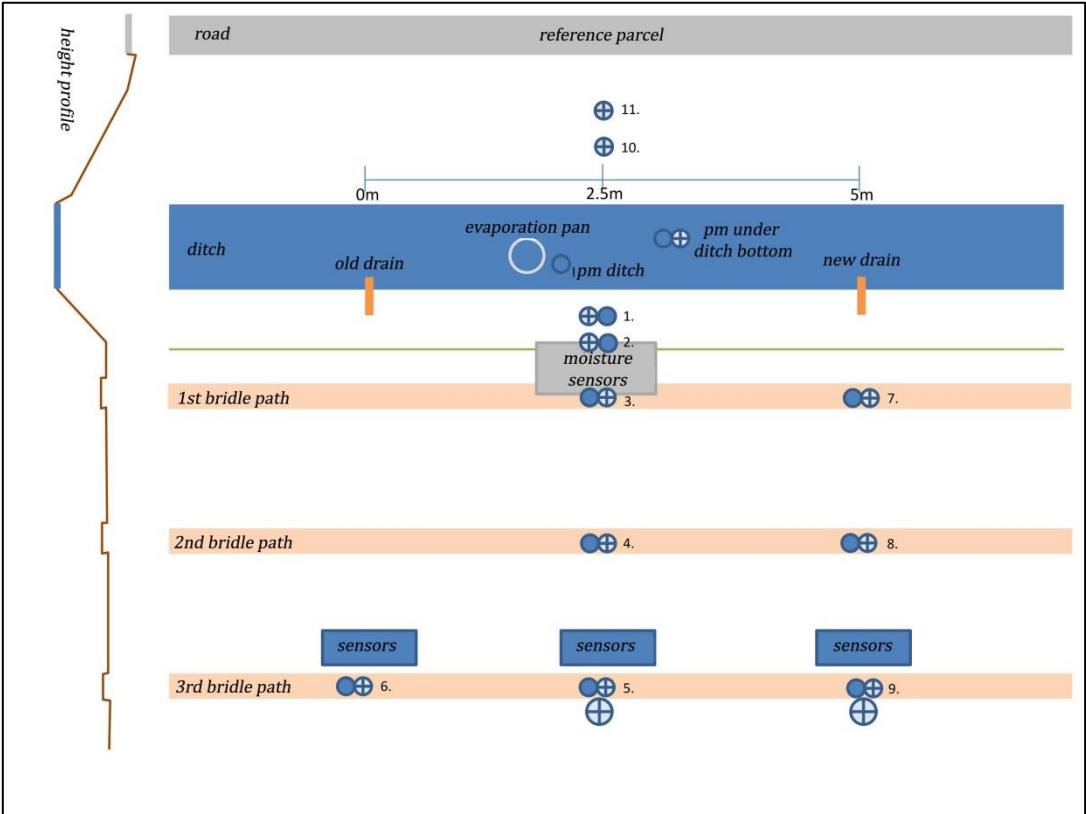


figure 5: Schematic measurement setup (source: personal communication, J. Delsman).

A number of piezometers were placed to get an insight into the groundwater heads. These heads are subject to precipitation, evaporation, seepage pressure and drainage. The piezometers were placed at and between tile drains at different distances from the ditch to get the best insights into the effect of the tile drains and the ditch. A few piezometers were also located in and at the other side of the ditch. The piezometers vary in length from 1 m to 2 m with a screen length of 0.20 m (figure 5). Automatic measurements of groundwater heads, EC values and temperature were obtained using (Schlumberger) pressure sensors. The following pressure sensors, or divers, were used (ACACIA WATER, 2013): (1) micro- or mini-divers which measure (water)pressure and temperature in piezometers, (2) baro-divers which measure the (air)pressure and temperature to compensate for the air pressure in water pressure values and (3) CTD-divers which measure (water)pressure, temperature and electrical conductance (EC) at the collection point of the drain discharge to measure the quality.

A clear outcome from the measurements is that the groundwater table is situated at the same level as, and is thus dominated by, the tile drains. Even after much rainfall, the groundwater table recuperates in a period of around 3 days. Moreover, the groundwater heads do not fall below the tile drains in dryer periods; probably due to the supply of seepage water from the subsurface. It should be mentioned that, during the monitoring period, much rain has fallen so a clear reaction to drought cannot be deduced. Another outcome from the measurements is that the effect of bulging between the two drains is limited to 5 cm, which is quite small. Likewise the influence of the ditch on the groundwater table is limited. In figure 6 and figure 7 an overview of the measured values of both the groundwater head and the EC measurements is given. The measurements of piezometer 5b and 9b are unrealistic; these were left out of the calibration process. Further observations are: (1) the clear reaction of the groundwater heads to the precipitation and (2) the high correspondence between the head values at different piezometers. This last effect is not present in the EC-values where there is a large variation between the different piezometers.

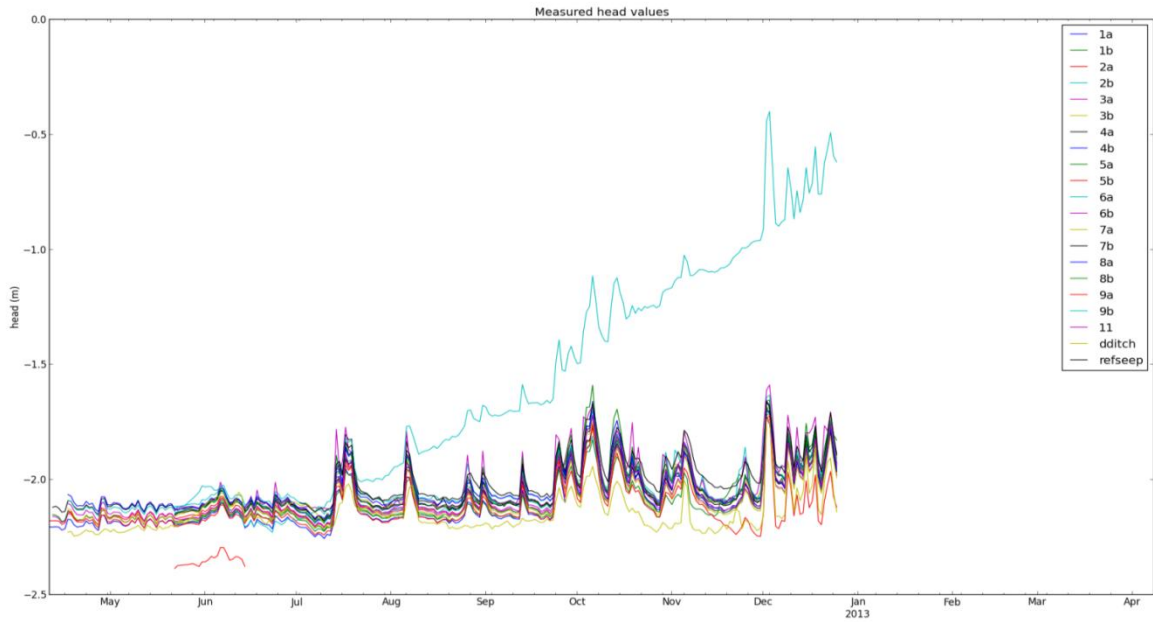


figure 6: Observed groundwater head values (source: own research).

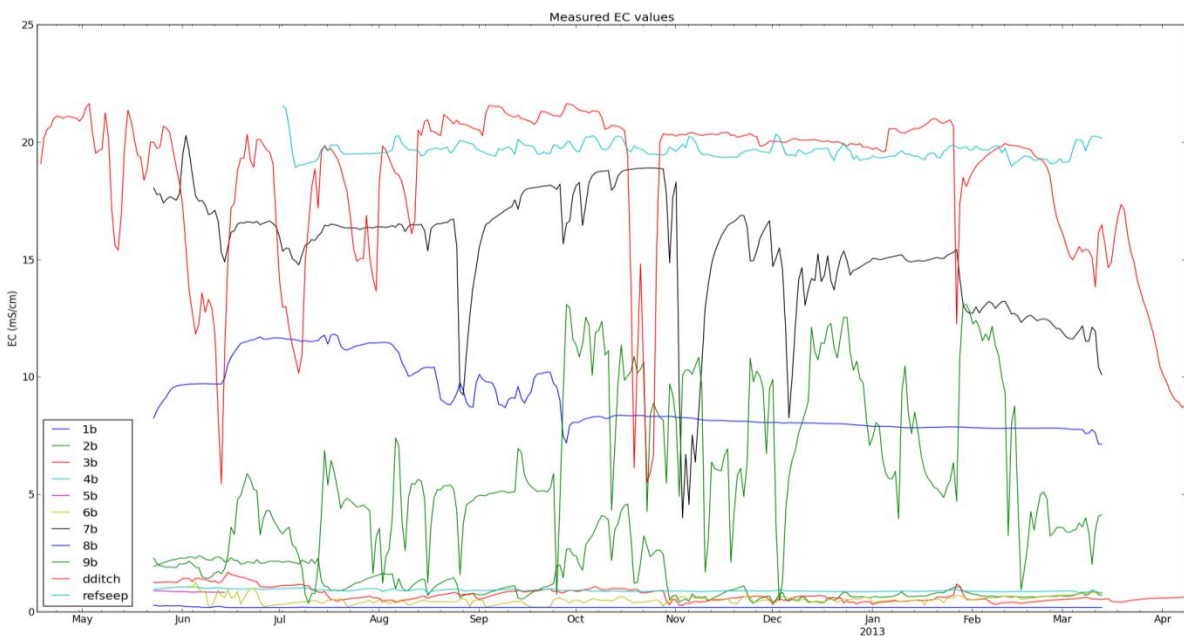


figure 7: Observed groundwater EC values (source: own research).

4.2.5 Tile drains

During the monitoring period, the discharge rate of the tile drains was measured (Itron flow-meter) together with the EC of this discharged water (CTD-diver). A comparison of the net precipitation during the period from 15 June to 1 October (122 mm), with the discharge of the drains during the same period (159 mm) shows that more water is drained than the theoretic groundwater recharge (net precipitation). This is an indication that the discharge of the drains not only consists of infiltrated precipitation, but also that around 30 % of the discharge is

derived from seepage water. This hypothesis is supported by the data that were retrieved from the CTD-diver. During the most part of the same period, the EC of the drained water was larger than 4 mS/cm; which is evidence that brackish water gets drained. Based on a salt mass balance for tile drains, an average flux of 0.28 mm/day was computed. In figure 8 the discharge and EC measurements are displayed. From mid-December to mid-April, the measurements were incorrect because one of the pumps in the system had broken down.

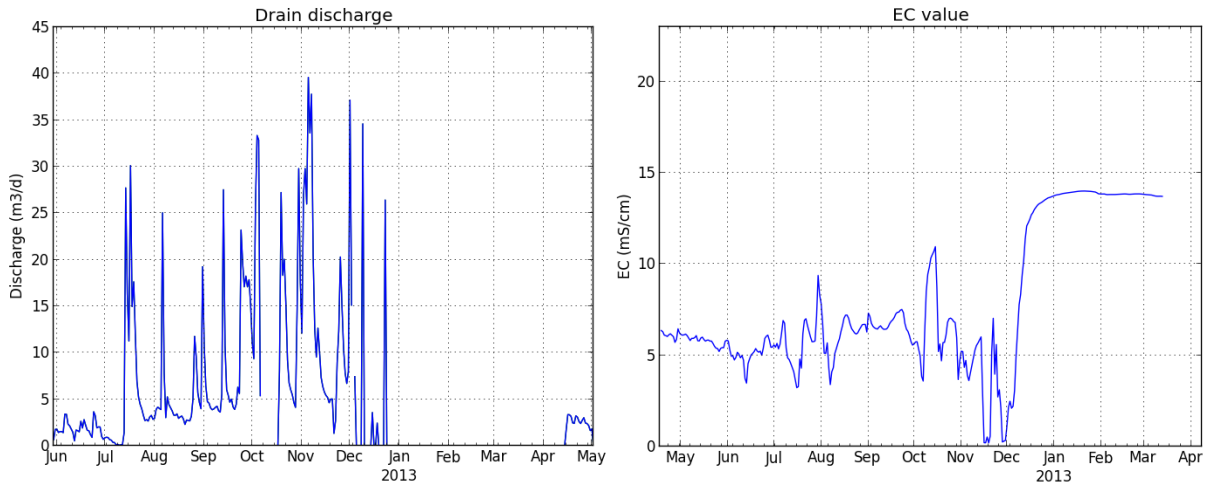


figure 8: (left) Observed drain discharge (source: own research). (right) Observed EC from drain discharge (source: own research).

4.2.6 Slug tests

In order to get a better insight in the hydraulic conductivity of the underground, we performed several slug tests by quickly subtracting a volume of water from the piezometer, and monitoring the change in groundwater head through time using a pressure sensor. Here the water present in the piezometers was pumped out, and a diver was inserted to measure the reaction of the groundwater head. To interpret the data, the Bouwer and Rice method was used. This method was chosen because it can be performed on screened wells that are partially penetrating (FETTER, 2001).

$$K = \frac{r_c^2 \ln\left(\frac{R_e}{R}\right)}{2L_e} \frac{1}{t} \ln\left(\frac{H_0}{H_t}\right) \quad (7)$$

Based on measurements from several piezometers, different saturated hydraulic conductivities were found, ranging from 0.4 to 0.9 m/d. Because the piezometer screens are located in the sand, these values are only applicable to the sands.

4.2.7 Temperature sensors

An array of regular temperature sensors was placed perpendicular to the ditch. These sensors measure the temperature every 15 minutes. Aside from these sensor data, there are also measurements of the temperature retrieved from some of the divers. figure 9 shows a global overview of the different temperature sensors for one specific time.

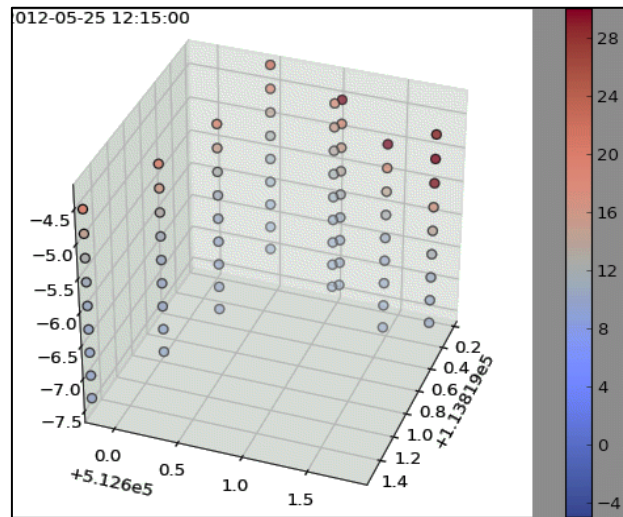


figure 9: 3D visualization of temperature variation on 25 May 2012, made with the temperature sensors (source: personal communication, J. Delsman).

4.3 Numerical modeling

This section elaborates on the numerical modeling. First the background of SEAWAT, the numerical code which is used in this study, is explained in detail, followed by a step by step explanation of the model properties.

4.3.1 Numerical code

For this study the numerical code SEAWAT is used. SEAWAT is a finite-difference computer code that combines MODFLOW (HARBAUGH, 2005; HARBAUGH, BANTA, HILL & MCDONALD, 2000; MCDONALD & HARBAUGH, 1988) and MT3DMS (ZHENG & WANG, 1999). Originally, SEAWAT was designed to simulate coupled variable-density groundwater flow and solute transport. It could already simulate transport of multiple species, yet the fluid density was calculated as a function of only a single species (e.g. salinity, chloride, or relative seawater fraction) (THORNE et al., 2006). In the original version it was already possible to approximate the heat transport, provided that: (1) temperature was the only species included in the simulation; and (2) the effect of temperature variation on fluid density was the only feedback on groundwater flow (meaning that the viscosity did not affect groundwater flow) (LANGEVIN et al., 2007).

In SEAWAT Version 4, released in 2007, two important new options are introduced: (1) the ability to solve the transport of energy and solutes simultaneously, and (2) the possibility for the fluid viscosity to vary (GUO & LANGEVIN, 2002; LANGEVIN et al., 2007; MA & ZHENG, 2010; THORNE et al., 2006). These functions are essential in the simulation of heat and salinity transport in a coastal aquifer. The fluid density and viscosity variations, due to changes in temperature and/or solutes, are represented in SEAWAT by the variable-density flow (vdf) process and viscosity (vsc) package (VANDENBOHEDE et al., 2011). These packages were simply added by exploiting the mathematical analogy between the advection-dispersion equation that describes the solute transport in three dimensions and the equation that deals with the 3D heat transport in groundwater flows (ANDERSON, 2005; LANGEVIN et al., 2010; THORNE et al., 2006; WANG & ANDERSON, 1982), as discussed in a previous chapter. The possibility to simulate solute and heat transport simultaneously is made possible by treating temperature as a different species in MT3DMS. This option, to enter different molecular diffusion coefficients for each species, became available with the release of MT3DMS version 5.2. (LANGEVIN et al., 2007; LANGEVIN et al., 2010).

Coupling groundwater flow to transport is primarily done through fluid density. In SEAWAT Version 4 the density is calculated as a function of solute concentration(s) and temperature. With this, the effect of viscosity variations can also be added through implementation of the relationship between permeability, viscosity and hydraulic conductivity. Viscosity is also function of both temperature and solute concentration (THORNE et al., 2006).

SEAWAT Version 4 has been tested extensively, which provides reasonable assurance that the physics of the system are represented accurately by the numerical approximations and implementation in the program (LANGEVIN et al., 2010). Most of these tests were standard variable-density benchmark problems, where density is a function of a single species. Examples of these benchmark problems can be found in GUO and LANGEVIN (2002), LANGEVIN, SHOEMAKER and GUO (2003) and LANGEVIN and GUO (2006). Some samples of the application of SEAWAT to simulate heat transport can be found in THORNE et al. (2006), DAUSMAN, LANGEVIN, THORNE and SUKOP (2009), LANGEVIN et al. (2010), VANDENBOHEDE et al.(2011), and many more.

Lastly, it should be mentioned that the SEAWAT code is not able to simulate heat transport in the unsaturated zone. However, this can be overcome partially by using a constant temperature boundary at the top of the model which represents the temperature at the water

table (VANDENBOHEDE et al., 2011). Another solution could be to model the problem in HYDROGEOSPHERE (TERRIEN, MCLAREN, SUDICKY & PARK, 2012) because this model can also incorporate the unsaturated zone. Yet for this study we opted to work with SEAWAT because: (1) the Deltares supervisor had experience working with this code, (2) SEAWAT needs less parameters and is faster, and (3) there is only a small unsaturated zone, characterized by small cracks.

4.3.2 *Model setup*

This section describes all properties that were used in the model, as they originated from field measurements, literature and multiple calibrations. For a summary, see Table 1.

4.3.2.1 *Grid properties*

In this study, the effects of the tile drains and the ditch are examined. Because the tile drains and the ditch are located perpendicular to each other, we opted to model the study-area in 3 dimensions. The length of the model is 110 m, representing the distance from the middle of the road on a dike until nearly the end of the parcel. The width of the model, which is 40 m, coincides with the part of the ditch that is isolated. For the thickness of the model 11.2 m is adopted, this implies 1.2 m from the top of the dike to the parcel and then 10 m below the parcel. The total thickness of the aquifer (25 m) was not modeled to maintain a good relationship between speed and accuracy. Because the full thickness is not modeled, the transmissivity is overestimated. This effect has been investigated, and it appears to have only a small impact. The mesh consisted of 60 columns of 1 m and 5 m, 54 rows of 0.75 m and 22 layers of 0.1 m to give a total of 71280 cells. Two various lengths, 1 m and 5 m, were used for the columns as another measure to enhance model efficiency. Smaller cells are modeled close to the ditch, while the larger cells are modeled further away into the parcel where high detail is not mandatory.

4.3.2.2 *Time properties*

The total simulation time spanned a period of 290 days. This was based on the measured precipitation and calculated evaporation values. To keep the model simple and efficient -even though most head, EC and temperature measurements are taken every 15 minutes- it was decided to subdivide the simulation period in stress periods of 1 day consisting of a single flow time step. To get a realistic starting concentration, the same period of 290 days with the same daily varying recharge and evaporation was repeated 12 times (3480 days), after which the transition zone, of fresh to salt water, had dropped to a stable level.

4.3.2.3 Ditch properties

The ditch is implemented through the MODFLOW river package (figure 10). The depth of the ditch is set at 1.2 m below the parcel, so 2.4 m below the top of the model. Yet only 0.1 m of water is present in the ditch, this value was kept constant throughout the execution of the model. The bottom of the river is 1.4 m wide and the slopes on both sides of the ditch correspond to 45 °, resulting in a width at the level of the parcel of 3.8 m. Finally the hydraulic resistance towards the ditch, which was put into the MODFLOW river package, was set to 0.05 days.

4.3.2.4 Drain properties

The tile drains were implemented perpendicular to the ditch at 1 m below the parcel, corresponding to 2.2 m below the top of the model, with the MODFLOW drain package. The drains are located to coincide with the model boundaries, and they are evenly distributed with an underlying spacing of 5 m. Within the width of the model, a total of 9 drains were implemented. Two sorts of drains were implemented intermittently, namely the old and the new drains. These correspond with a conductance of 0.24 m²/d and 0.4 m²/d. The two drains at the model boundaries were implemented with only half their conductance as a solution to the reflective effect of the model boundaries.

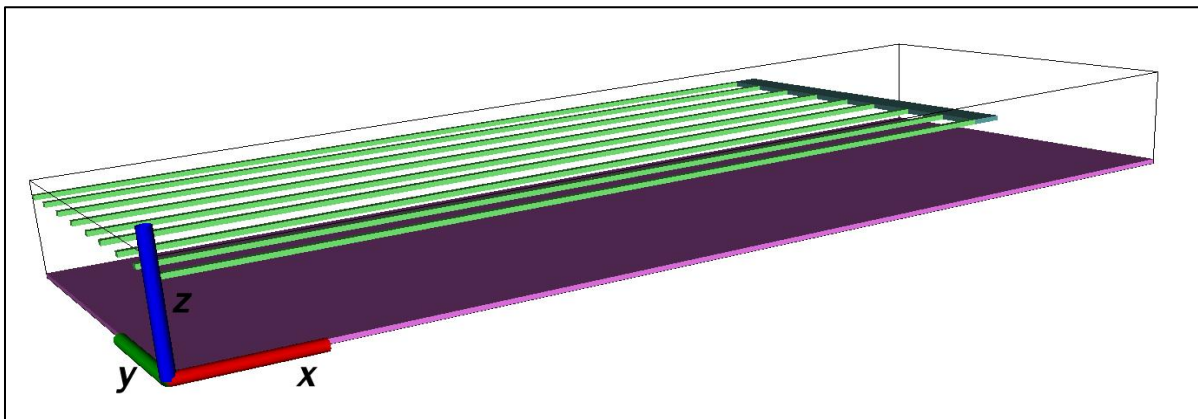


figure 10: Model schematization, showing the ditch (blue), the different tile drains (green) and a screen of wells (pink) (source: own research).

4.3.2.5 Seepage properties

Like described in the field measurements, a local seepage flux of 0.28 mm/d was calculated. Because the seepage flux is known, while there is little to no information about the evolution of groundwater heads in the deeper underground (only one deeper piezometer, which is only 4 m deep), it was opted to simulate the seepage with the MODFLOW well package. In this

situation the entire bottom layer of the model is filled with well-cells in order to let the flux, which is kept constant throughout the whole simulation period, get into the model.

4.3.2.6 Underground properties

Based on the information from the investigation drillings, the underground is subdivided into two lithological strata. The first 0.3 m is modeled as clay, while the rest of the underground is presumed to be sand.

- Clay lithology

The vertical hydraulic conductivity of the clay is set to 0.0007 m/d, based on an earlier study made in the same study area (MARGARITA, 2012). Based on model calibrations, the anisotropy (ratio of horizontal hydraulic conductivity to vertical hydraulic conductivity) is set to 6.45. The cell wetting and drying option from MODFLOW was used to simulate the moving water table. The primary storage capacity was used where a cell is confined throughout the course of a simulation. However, if the water level was below the top of a cell during a simulation, then the cell is under a water-table condition, and a specific yield parameter is used instead of the storage capacity. The confined storage capacity used for the clay was fixed to $1e^{-3}$, while the specific yield was set to 0.12. By using the specific yield parameter to simulate the moving water table, the model was simplified in comparison to the actual field, as it does not take into account the dynamic conditions in the unsaturated zone. A solution could be to model the problem in HYDROGEOSPHERE. For the porosity of the clay a value of 0.38 was assigned.

- Sand lithology

The vertical hydraulic conductivity of the sand was set to 0.34 m/d, with the anisotropy set to 1.82 to get to a horizontal hydraulic conductivity of 0.65 m/d. The storage capacity and the specific yield were set to $1e^{-3}$ and 0.20 respectively. For the porosity of the sand the same standard value of 0.38 was taken.

4.3.2.7 Solute transport properties

We opted to use ECs (mS/cm) to represent density differences in the model, similar to the method used by POST (2011), because all measurements of solutes were made in ECs. Based on model calibrations, the longitudinal dispersivity was set to a value of 0.41 m, the horizontal transverse dispersivity to a value of 0.041 m and ultimately the vertical transverse dispersivity was set to 0.0041 m. The molecular diffusion coefficient was assumed to be $1e^{-5}$ m²/d. Additionally for the fluid properties, the reference density was set to 1000 kg/m³ and the

approximate change in density over the change in EC was set to 0.4486. This last value was calculated with the UNESCO 1980 equation of state (POST, 2011).

4.3.2.8 Heat transport properties

The change in density over the change in temperature was set to $-0.375 \text{ kg/m}^3\text{°C}$, this value comes from the SEAWAT guidebook (LANGEVIN et al., 2010). Furthermore, constant values were chosen for the bulk thermal diffusivity and the distribution coefficient for temperature, namely $0.15 \text{ m}^2/\text{d}$ and $2e^{-4} \text{ m}^3/\text{kg}$. Within the timeframe of this internship it has not been possible to make a working model whereby heat transport is taken into consideration. Therefore, all the heat transport parameters are hypothetical and the applicability cannot be guaranteed.

4.3.2.9 Boundary conditions

The 4 model boundaries were all set to be no flow boundaries. Two of them are where the tile drains are located; by placing these on the borders a water divide is created which acts as a no flow boundary. The road on top of the dike also acts as a water divide, because at the other side of the road the same situation is present, namely a ditch and after that a parcel. The last – and furthest – side of the parcel is less known. Assuming this side is a no flow boundary is a simplification. This is no problem because we are only interested in the interactions towards the ditch, and this boundary is chosen far enough (to have no influence).

Inflow is possible as precipitation, seepage and interaction with the ditch. An EC value of 0 mS/cm and a temperature of 10 °C were assigned to the water entering the system as precipitation. The seepage water received an EC of 22 mS/cm and a temperature of 11 °C . Likewise, the ditchwater received an EC of 0.2 mS/cm and a temperature of 11 °C . All these starting concentrations, ECs and temperatures, were approximations based on the field measurements. Water could leave the system by tile drainage, evaporation and also by the interaction with the ditch. The evaporation water was assigned an EC value of 0 mS/cm and a temperature equal to the current groundwater in the top layer.

Table 1: Input values for the model.

		Input parameter	Value	Unit	Comments	
Grid properties		Length x	110	m	Field measurements	
		Length y	40	m	Field measurements	
		Length z	11.2	m	Field measurements	
		Number of columns	60	-	Field measurements	
		Number of rows	54	-	Field measurements	
		Number of layers	22	-	Field measurements	
		Dx1	1	m	Field measurements	
		Dx2	5	m	Field measurements	
		Dy	0.75	m	Field measurements	
	Dz	0.5	m	Field measurements		
Time prop		Nper	290	d	Field measurements	
		Nstp	1	d	Field measurements	
		Perlen	1	d	Field measurements	
Ditch properties		Depth	2.4	m	Field measurements	
		Bottom width	1.4	m	Field measurements	
		Waterheight	0.1	m	Field measurements	
		Slope	45	°	Field measurements	
		Hydraulic resistance	0.05	d	Calibration	
Drain properties		Depth	2.2	m	Field measurements	
		Spacing	5	m	Field measurements	
		Conductance old drain	0.24	m ² /d	Calibration	
		Conductance new drain	0.4	m ² /d	Calibration	
Seepage properties		Seepage flux	0.28	mm/d	Field measurements	
Underground properties	clay	Clay depth	0.3	m	Field measurements	
		Vertical hydraulic conductivity	0.0007	m/d	Literature	
		Anisotropy	6.45	-	Calibration	
		Storage capacity	1e ⁻³	-	Calibration	
		Specific yield	0.12	-	Calibration	
	sand	Porosity	0.38	-	Calibration	
		Vertical hydraulic conductivity	0.34	m/d	Calibration	
		Anisotropy	1.82	-	Calibration	
		Storage capacity	1e ⁻³	-	Calibration	
		Specific yield	0.20	-	Calibration	
		Porosity	0.38	-	Calibration	
		Solute transport properties	Longitudinal dispersivity	0.41	m	Calibration
			Molecular diffusion coefficient	1e ⁻⁵	m ² /d	Calibration
			Reference density	1000	kg/m ³	Field measurements
Fluid density-solute relationship	0.4486		-	Literature		
Heat transport prop	Fluid density-heat relationship	-0.375	kg/m ³ °C	Literature		
	Bulk thermal diffusivity	0.15	m ² /d	Literature		
	Distribution coefficient	2e ⁻⁴	m ³ /kg	Literature		
Boundary conditions	Recharge concentration	0	mS/cm	Field measurements		
		10	°C	Field measurements		
	Seepage water concentration	22	mS/cm	Field measurements		
		11	°C	Field measurements		
	Ditch concentration	0.2	mS/cm	Field measurements		
		11	°C	Field measurements		
	Evaporation concentration	0	mS/cm	Field measurements		

4.4 Model calibration

The model was calibrated in two different manners, used simultaneously: (1) manually by adjusting parameters based on visual interpretation of the fit between simulated and measured values, and (2) by using Model-Independent Parameter Estimation and Uncertainty Analysis (PEST) where the model parameters are adjusted in order to minimize the discrepancies between the model-generated data and the corresponding measurements. PEST is able to do this by taking control of the model and running it until an optimal set of parameters is found. As this does not take into account optimal interpretation (a good model fit with unrealistic parameters), the combination of PEST and manual calibration turned out to be a great solution. For more information about PEST, we refer to the user manual (WATERMARK NUMERICAL COMPUTING, 2010).

The Nash-Sutcliffe coefficient (NSC), the least squares fit (LSQ) and the mean value (MV) were calculated for the head and EC values from the different piezometers, for the drain discharge rate and for the ECs from the drained water. The NSC and LSQ were calculated for a period where the observations have a high reliability, from 30 May 2012 until 11 October 2012 (135 days).

$$\text{NSC} = 1 - \frac{\sum_{t=1}^n (o_t - s_t)^2}{\sum_{t=1}^n (o_t - \bar{o})^2} \quad \text{LSQ} = \sum_{t=1}^n (o_t - s_t)^2 \quad \text{MV} = \bar{s} \quad (8)$$

The NSC can range from $-\infty$ to 1. A perfect match corresponds to a coefficient of 1. Furthermore, an NSC of 0 indicates that the model predictions are as accurate as the mean of the observed data, whereas it being less than 0 occurs when the observed mean is a better predictor than the model. For the LSQ, the value can range from $+\infty$ to 0, where an LSQ of 0 corresponds to a perfect match. Finally the aim of the MV is to bring the average of the measured and calculated values as close as possible to each other.

5 RESULTS

This chapter summarizes the results that came out of the last model run, incorporating groundwater flow and solute transport. Within the framework of this internship it was not possible to successfully incorporate heat transport. Model convergence could not be accomplished using the heat transport properties specified earlier; further research is needed to identify possible errors in the heat transport settings.

5.1 Calibration

5.1.1 Head

figure 11 shows the measured and modeled values of the groundwater head in piezometer 5a together with the precipitation to get a clear insight into the interactions. Piezometer 5a was taken as a representative of the majority of piezometers. It is clear that the model reacts in a similar manner to the precipitation as the observed values, although the observations seem to respond more sharply. Also included in figure 11 are two boxplots that give information about the LSQ and NSC of all piezometers. Overall the observed and modeled values of piezometer 5a show a good fit, this translates into a NSC of 0.50 and a LSQ of 0.65. When examining all the piezometers, the NSC varies from -4.24 to 0.69 and the LSQ from 128 to 3.41. To give an idea of the deviation, the average LSQ of all piezometers -in the 135 days for which the model calibration coefficients were calculated- is equal to 1.28, this results in an average error of 0.09737 m per measurement.

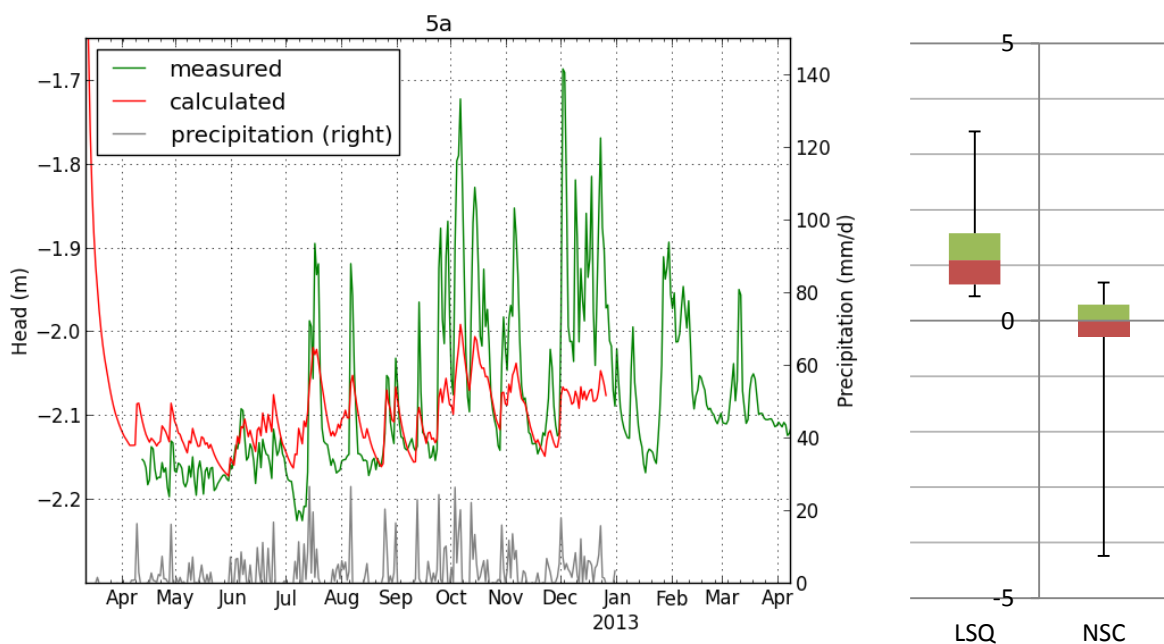


figure 11: (left) plot of the measured and modeled groundwater head for piezometer 5a, with the indication of the precipitation. (right) Boxplots showing the variation of the LSQ and NSC values of all piezometers (source: own research).

5.1.2 Salinity

As shown in figure 12, where the EC of piezometer 4a and two descriptive boxplots are shown, the matching of measured and modeled EC shows no clear fit. This results in a NSC score ranging from -2395027.51 to -8.51 and a LSQ score ranging from 924.66 to 47075.5.

With an average LSQ of 19516.26, the average error lies in the order of 12.02 mS/cm per measurement.

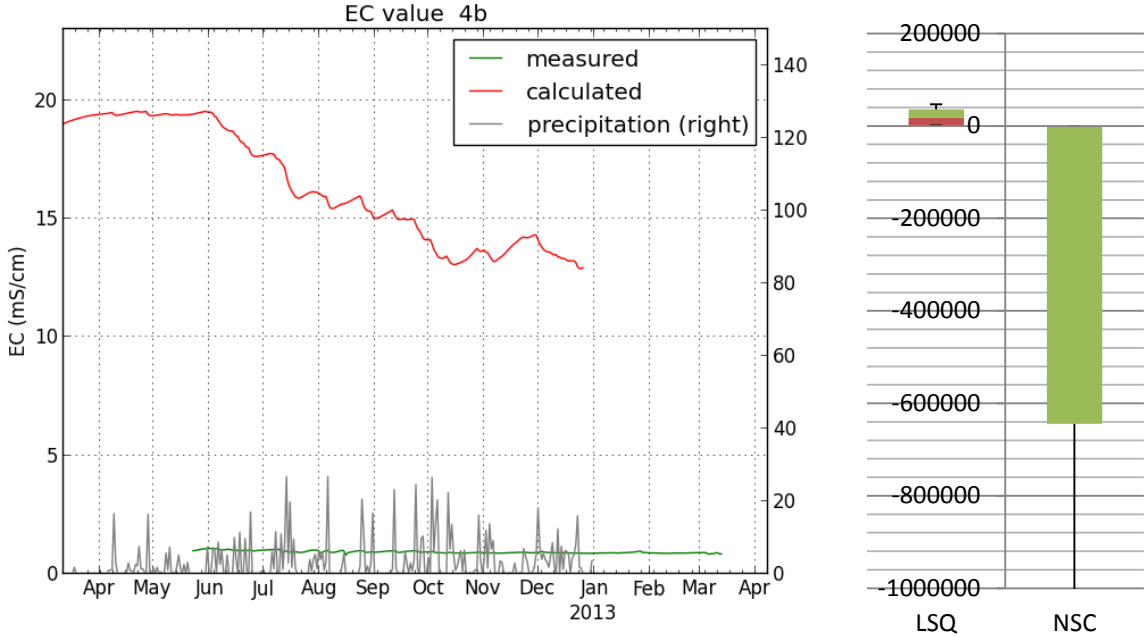


figure 12: (left) plot of the measured and modeled EC values for piezometer 4b, with the indication of the precipitation. (right) Boxplots showing the variation of the LSQ and NSC values of all piezometers (source: own research).

5.1.3 *Tile drain*

Figure 13 shows the modeled and observed drain discharge, while figure 14 shows the measured and modeled EC of this discharge. Even though the fit is far from perfect, it is still clear that the modeled and measured values show a high resemblance. This leads to an NSC of 0.08 for the drain discharge and -0.16 for the EC, while the LSQ values are 13875.69 and 817.25 respectively. Another observation is the reaction to the precipitation. figure 14 clearly indicates the response to precipitation. After a precipitation-event, the ECs of the drained water drop instantaneously. Subsequently, a slow but steady rise of ECs is detected. This effect is observable in both the measured and the modeled values, although the effect is more pronounced in the model.

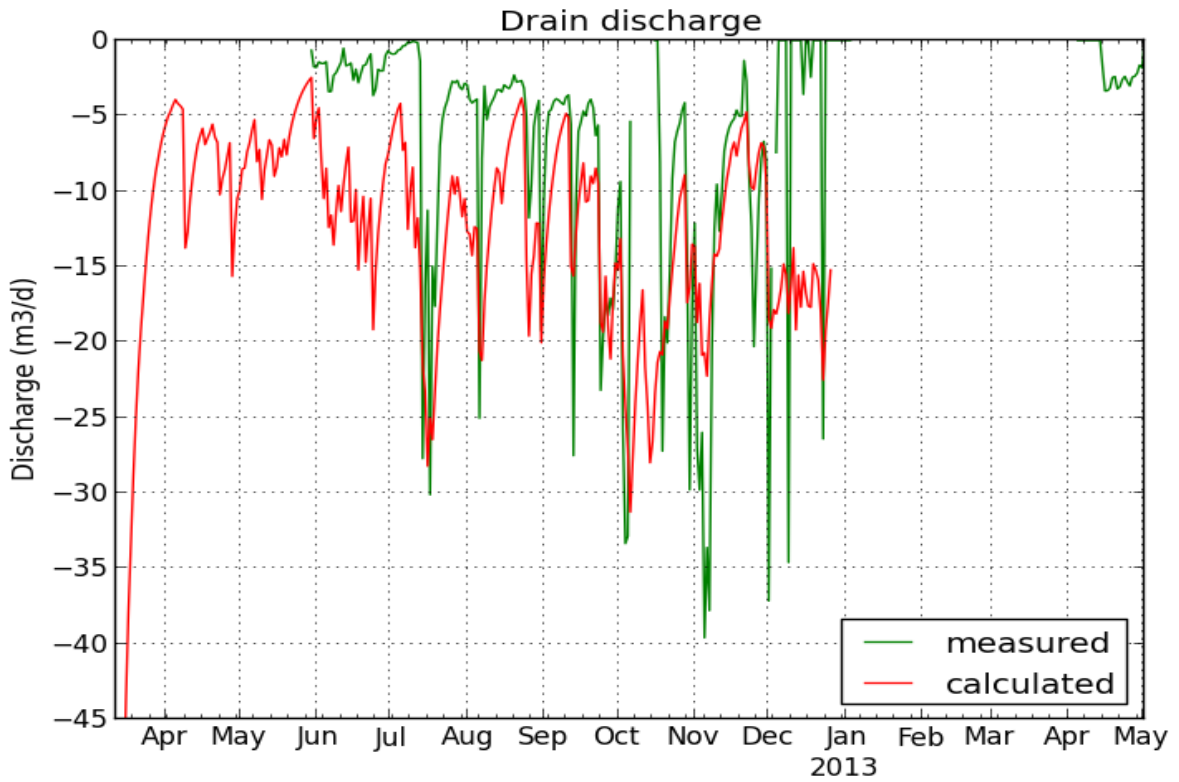


figure 13: Measured and modeled drain discharge (source: own research).

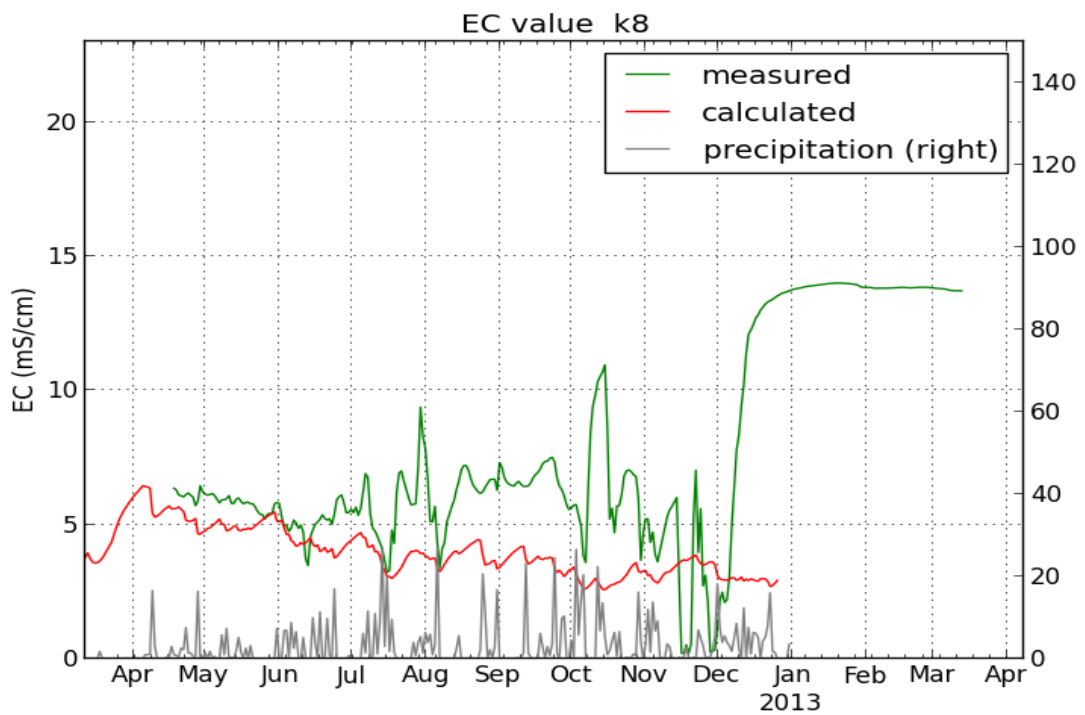


figure 14: Measured and modeled EC of the drain discharge. k8 stands for klico8, which is the name of the container where the drain discharge is collected (source: own research).

5.2 Distribution

5.2.1 Groundwater head

figure 15 shows a cross-section through the model in the x-direction (length of the parcel). The lowest heads are observed at the ditch; with a constant head value of -2.30 m (fixed water level of the ditch). At the side of the parcel, the head values fluctuate slightly above the level of the drains (-2.05 m), and there is not much variation in depth. This is in contrast to the other side of the ditch, where no drains are installed. Here the groundwater heads rise significantly higher and have more variation with depth. The effect of the drains becomes even more evident in figure 16; this figure shows a cross-section in the y-direction (width of the parcel). One can observe the lower heads at the position of the tile drains, and the difference between the new and the old drains. Also, the head difference between locations on and between drains is around 0.05 m, which corresponds with the field measurements. White cells in both figures represent inactive cells. A somewhat peculiar situation occurs in the upper right corner of figure 15, where the cells below a single active cell are already inactive. This is because the active cell is modeled as clay, which remains active for a longer period after precipitation since it drains slowly, yet the underlying cells drain more easily as they are modeled as sand.

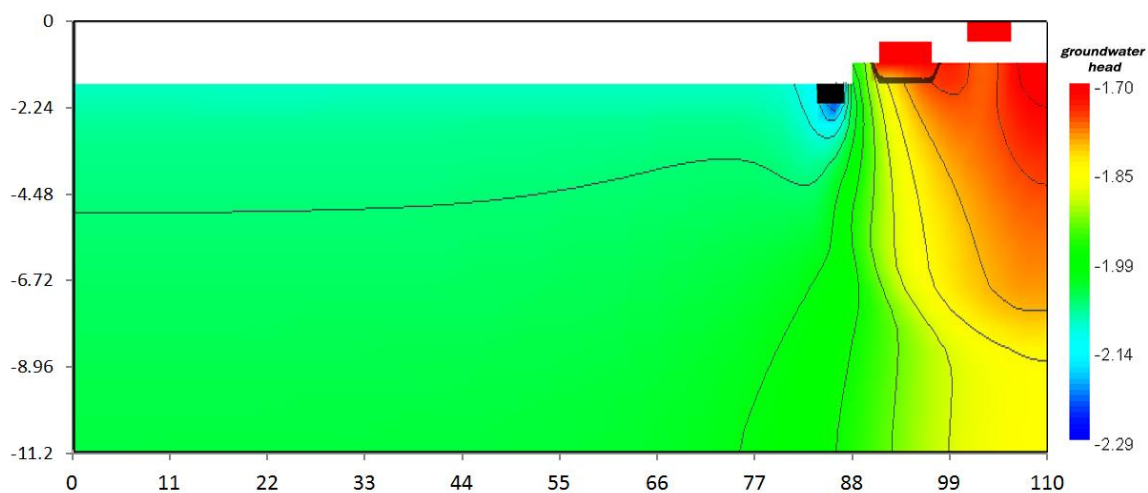


figure 15: Model cross-section showing groundwater heads and isosurfaces, perpendicular to the ditch. The ditch is shown in black (source: own research).

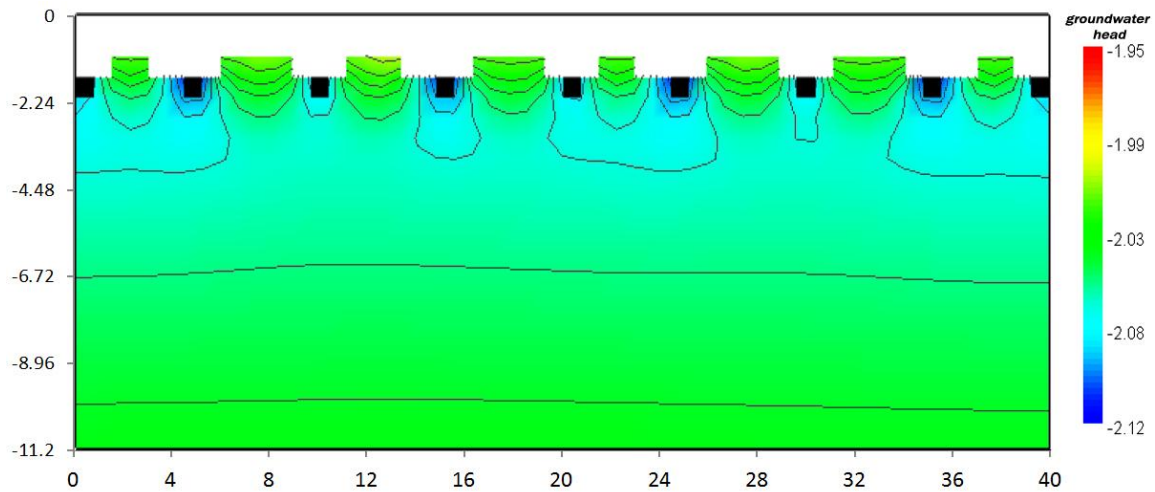


figure 16: Model cross-section showing groundwater heads and isosurfaces, parallel to the ditch. The drains are shown in black (source: own research).

5.2.2 Salinity

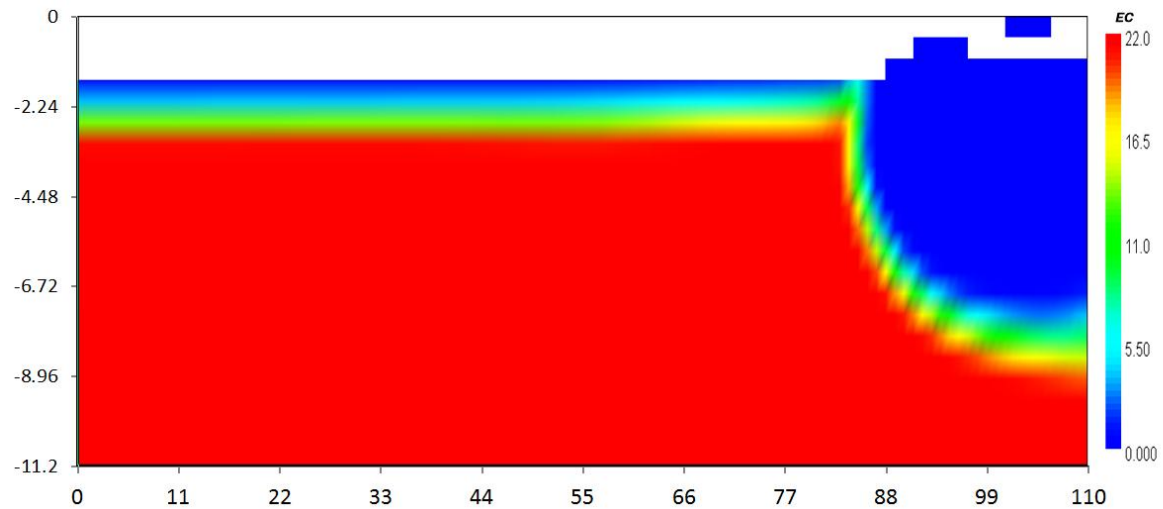


figure 17: Model cross-section showing EC, perpendicular to the ditch (source: own research).

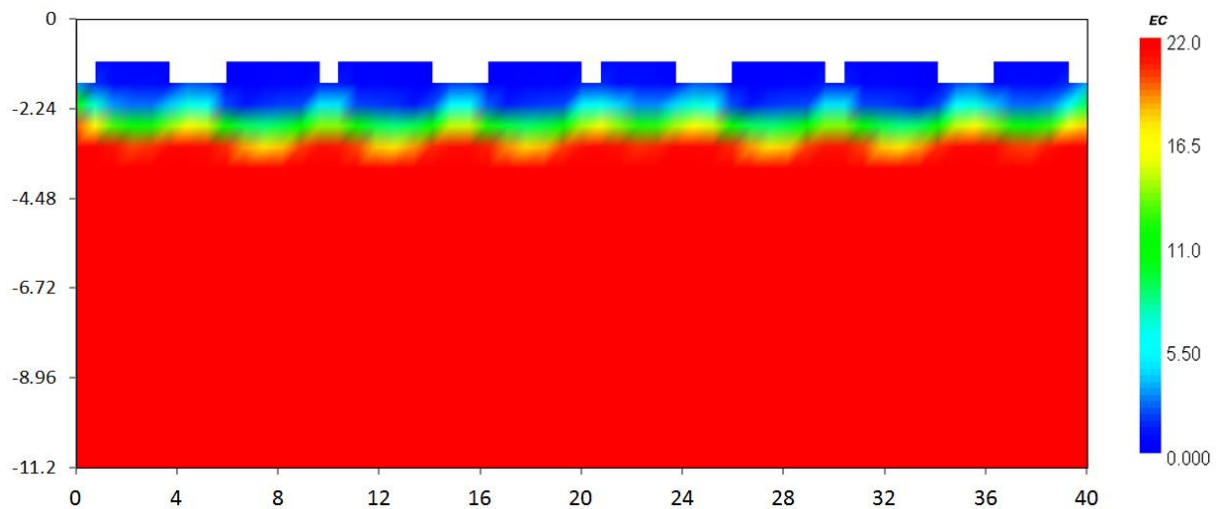


figure 18: Model cross-section showing EC, parallel to the ditch (source: own research).

figure 17 and figure 18 show the same cross-sections as in the previous chapter, yet this time the EC-values are visualized. Ffigure 18 shows many similarities with the CVES that was made, although the modeled location of the fresh to salt transition zone appears to be higher. Also, the difference in drainage capacity between the old and the new tile drains seems to be less pronounced. Another remarkable observation is the fresh-water lens at the side of the road.

6 DISCUSSION

6.1 Groundwater- and solute transport towards ditch and drains

Based on the results, we get a clear insight in how groundwater and solutes flow. There are well-marked differences between the two sides separated by the ditch. At the side of the parcel, the head values do not know much variation with the depth. Also, below -3.5 m, the groundwater flow is pointed upwards with nearly no horizontal displacement. Above -3.5 m the drains act on the groundwater flow: (1) between the drains, where bulging up to 0.05 m is observed, the groundwater flows downwards and thus precipitation can infiltrate and (2) on the drains, where the groundwater flow is drawn towards the drain, attracting deeper seepage water and infiltrated precipitation. This also explains the relatively shallow location of the fresh to salt transition zone (figure 18); the fresh water cannot infiltrate much deeper than the level of the drains. At the side of the road the situation is completely different. The groundwater flows downwards with a high horizontal displacement towards the ditch, therefore the fresh precipitation water gets the chance to infiltrate deeper, forming a fresh-water lens. Finally the groundwater that enters the ditch directly as opposed to by drains, mainly originates from the side of the road, and is thus relatively fresh water.

6.2 Interactions to precipitation

The model reacts in a similar manner to the precipitation as the measured values, as can be seen in both the head calibration and the EC of the drain discharge (figure 11 and figure 14). Yet in both situations the observations show a sharper response in comparison to the modeled values. This effect may be derived from: (1) imperfections in the model, measurement errors and slightly off parameters, (2) flattening of the precipitation input and (3) because the unsaturated zone is not considered.

In case of model imperfections, measurement errors and slightly off parameters, the storage capacity is modeled too high in comparison to reality. This may be due to an overestimation

of resistance in the model, an incorrect storage capacity or specific yield, etc. The flattening of the precipitation has the certain effect that the modeled values become more spread out, yet this does not explain why the modeled values have a greater spread throughout the whole simulation period. We would expect this after high precipitation events only. Lastly there is the effect of the unsaturated zone which is not modeled. Normally a portion of the precipitation water is contained in the unsaturated zone, after which it slowly infiltrates towards the groundwater. Here, with the unsaturated zone not modeled, the precipitation is put directly into the groundwater, resulting in an instant head difference. We would expect this to lead to sharper reactions after precipitation, but remarkably the opposite occurs. This could be explained by the capillary-fringe phenomenon, whereby the moisture content in the unsaturated zone is almost saturated. This implies that very fast groundwater head changes occur after adding or subtracting small amounts of water. Because the study area consists of clayey grounds, this phenomenon is a real possibility which should be investigated further. Unfortunately this cannot be modeled without incorporating the unsaturated zone.

6.3 EC measurements

The model calibration shows a big difference between the ECs from the piezometers (mean NSC of -409324.51 and mean LSQ of 19516.26) as compared to the ECs of the drain discharge (NSC of -0.16 and LSQ of 817.25). It is self-evident that an error like the ECs from the piezometers is inadmissible. One possibility is that (part of) the problem comes from the measurements. The water in a piezometer experiences various effects which have their influence on the measured EC, yet this relationship was not taken into consideration. However, the main source of errors is derived from the model discretization. As previously illustrated in the field measurements, the EC observations know a large variation between the different piezometers, while the head values know almost no variation. This is an indication that the EC measurements are more sensitive to local variations in the subsurface, yet the model was only discretized in clay and sand with no further local subdivisions. This also explains why the modeled EC of the drain discharge shows a better fit with the observations; the drainage water from an entire area is collected so the local variations are less evident in the observations. Finally, it is complex to model solute transport: a small variation of the fresh-salt transition zone has a huge effect on the local EC values. For example, the position of the fresh-salt transition zone knows little variation throughout the simulation period (order of centimeters), yet the EC of the drain discharge shows significant fluctuation.

6.4 Utility of adding solute transport

The results shown in the previous part are all from the last run, where solute transport is incorporated into the model. Several steps had been taken to get to these results: the formation of an initial conceptual model, the modeling of groundwater flow with standardized parameters, the use of manual calibration and PEST to find more applicable parameters, adding solute transport to the model and again calibrating etc... What is important to point out here, is the first stage consisted of forming a robust model with only groundwater flow; solute transport was left for later. In this stage of the internship the model showed a good fit to the groundwater head observations. After the addition of solute transport to the model, it became clear that the first set of parameters could not lead to a good fit of the observed and measured EC-values of the drain discharge, at least not without adjusting the parameters beyond their physical realistic boundaries. This made the EC an important additional constraint in the search for optimal parameters. Eventually another set of parameters was found, which proved a better model fit to both the groundwater head measurements and the EC measurements of the drain discharge. Regrettably it was not possible to describe this statistically; this could be an interesting direction for further research.

6.5 Heat transport

Unfortunately heat transport could not be incorporated successfully within the framework of this internship. Discussion with J. Claus, J. Delsman, L. Lebbe, G. Oude Essink and A. Vandenbohede revealed that problems with heat transport are common and not easy to overcome. One bypass was proposed, namely using the “mass-loading source” option in the MT3DMS Source and Sink Mixing (ssm) Package. Instead of the recharge having a certain temperature, a known volume of water is pumped into the uppermost active cell and immediately afterwards extracted again. By supplying the pumped and the extracted water with different temperatures, a certain amount of energy is added to the model. By varying the pumped volume and the temperature difference, the temperature variations caused by the recharge can be mimicked. Because the wetting and drying option is used in this model, the drawback of this technique is that the uppermost active cell has no constant location. Therefore it has not been possible to apply this technique successfully before the end of the internship period. It is well worth the consideration to still apply this technique in a further step of this study. Another possibility exists in the use of HYDROGEOSPHERE (THERRIEN et al., 2012) whereby the unsaturated zone can be incorporated into the model.

7 CONCLUSION

For this internship, the objective was to incorporate head, concentration and temperature measurements in an inverse model to be used to estimate flow patterns to an agricultural ditch in the Netherlands. From the study area a multitude of measurements was taken in the context of Project 2.1: meteorological measurements, investigation drillings, CVES, head measurements, EC measurements, discharge measurements, slug tests and temperature measurements. These measurements were used to develop and optimize the numerical model. Unfortunately it was not possible to succeed for all objectives within the timeframe provided in this internship, in particular the incorporation of heat transport. Nevertheless some interesting conclusions can be drawn at the end of this internship.

First off, the model gives a clear insight in how groundwater and solutes flow within the study area, and how the system interacts to precipitation. Secondly the incorporation of solute transport proved to be an important additional constraint in the calibration towards optimal parameters, though modeling solute transport remained difficult and caution is recommended. And finally, even though finalization was not possible within the timeframe of this internship, the foundations are laid to incorporate heat transport in a future stage.

For further studies it could prove wise to use HYDROGEOSPHERE instead of SEAWAT, especially since there are indications that the unsaturated zone has an important influence on the measurements taken in the study area.

8 REFERENCES

- ACACIA WATER (2011). SKB Project-voorstel: Alternatieve vormen van duurzaam bodemgebruik en waterbeheer door en voor agrariërs. Kenmerk: F20110365.
- ACACIA WATER (2013). SKB Project-voorstel: Alternatieve vormen van duurzaam bodemgebruik en waterbeheer door en voor agrariërs. Kenmerk: F2013413.
- ANDERSON, M.P. (2005). Heat as a GroundWater Tracer. *Ground Water* 43(6), 951-968.
- ANDREWS, C.B. & ANDERSON, M.P. (1979). Thermal alteration of groundwater caused by seepage from a cooling lake. *Water Resources Research* 15(3), 595– 602.
- BAYER, P., GIRALDO, N.M., MENDEZ, J.H., RASUOLI, P., ZHENG, C., BLUM, P. (2008). Heat transport modeling using MODFLOW/MT3DMS. *MODFLOW and More 2008: Ground Water and Public Policy–Conference Proceedings*.
- BEAR, J. (1972). Dynamics of Fluids in Porous Media. *American Elsevier Publishing Company Inc*.
- BECK, A.E., GARVEN, G., STEGENA, L. (1989). Hydrogeological regimes and their subsurface thermal effects. *Geophysical Monograph* 47, 158 pp.
- BECKER, M.W. (2006). Potential for satellite remote sensing of ground water. *Ground Water* 44(2), 306-318.
- BENSE, V.F. & KOOI, H. (2004). Temporal and spatial variations of shallow subsurface temperature as a record of lateral variations in groundwater flow. *Journal of Geophysical Research* 109, 13 pp.
- BRAVO, H;R;, JIANG, F., HUNT, R.J. (2002). Using groundwater temperature data to constrain parameter estimation in a groundwater flow model of a wetland system. *Water Resources Research* 38(8).
- BREDEHOEFT, J.D. & PAPADOPULOS, I.S. (1965). Rates of vertical groundwater movement estimated from the Earth's thermal profile. *Water Resources Research* 1(2), 325– 328.
- BUNDSCHUH, J. (1993). Modeling annual variations of spring and groundwater temperatures associated with shallow aquifer systems. *Journal of Hydrology* 142, 427– 444.

- CONSTANTZ, J. (2008). Heat as a tracer to determine streambed water exchanges. *Water Resources Research* 44, 20 pp.
- CONSTANTZ, J., COX, M.H., SU, G.W. (2003). Comparison of heat and bromides as ground water tracers near streams. *Ground Water* 41(5), 647–656.
- CONSTANTZ, J., THOMAS, C.L., ZELLWEGER, G. (1994). Influence of diurnal variations in stream temperature on streamflow loss and groundwater recharge. *Water Resources Research* 30(12), 3253–3264.
- DAUSMAN, A.M., LANGEVIN, C.D., THORNE, D.T., SUKOP, M.S. (2009). Application of SEAWAT to Select Variable-density and Viscosity Problems. *USGS Scientific Investigations Report 2009-5028*, 41 pp.
- DE LOUW, P.G.B., EEMAN, S., SIEMON, B., VOORTMAN, B.R., GUNNINK, J., VAN BAAREN, E.S., OUDE ESSINK, G.H.P. (2011). Shallow rainwater lenses in deltaic areas with saline seepage. *Hydrology and Earth System Sciences* 15, 3659-3678.
- DE LOUW, P.G.B., GRIFFIOEN, J., VAN DEN EERTWEGH, G.A.P.H. (2000). High nutrient and chloride loads to surface water in polder areas due to groundwater seepage. *Past Achievements and Future Challenges*. 418–486.
- DE LOUW, P.G.B., OUDE ESSINK, G.H.P., GOES, B.J.M., SERGI, F. (2008). Characterization of local rainwater lenses in agricultural areas with upward saline seepage: monitoring results. *Salt water intrusion meeting, Naples, Florida*.
- DE LOUW, P.G.B., OUDE ESSINK, G.H.P., STUYFZAND, P.J., VAN DER ZEE, S.E.A.T.M. (2010). Upward groundwater flow in boils as the dominant mechanism of salinization in deep polders, The Netherlands. *Journal of Hydrology* 394, 494-506.
- DEMARSILY, G. (1986). Quantitative Hydrogeology. *Academic Press*, 464 pp.
- FERGUSON, G. (2007). Heterogeneity and thermal modeling of ground water. *Ground Water* 45(4), 485–490.
- FETTER, C.W. (2001). Applied Hydrogeology, Fourth Edition, Prentice Hall, New Jersey.
- GELHAR, L.W., WELTY, C., REHFELDT, K.R. (1992). A critical review of data on field-scale dispersion in aquifers. *Water Resources Research* 28(7), 1955–1974.

- GRESKOWIAK, J., PROMMER, H., MASSMANN, G., NÜTZMANN, G. (2006). Modeling Seasonal Redox Dynamics and the Corresponding Fate of the Pharmaceutical Residue Phenazone During Artificial Recharge of Groundwater. *Environmental Science & Technology* 40(21), 6615–6621.
- GUO, W. & LANGEVIN, C.D. (2002). User's Guide to SEAWAT: A Computer Program for Simulation of Three Dimensional Variable-Density Ground-Water Flow. *U.S. Geological Survey Techniques and Methods* 6(A7), 87 pp.
- HARBAUGH, A.W. (2005). MODFLOW-2005, The U.S. Geological Survey Modular Ground-Water Model—the Ground-Water Flow Process. *U.S. Geological Survey Techniques and Methods* 6(A16), 253 pp.
- HARBAUGH, A.W., BANTA, E.R., HILL, M.C., MCDONALD, M.G. (2000). MODFLOW-2000, The U.S. Geological Survey modular ground-water model—User guide to modularization concepts and the ground-water flow process. *USGS Open- File Report* 00-92, 121 pp.
- HATCH, C.E., FISHER, A.T., REVENAUGH, J.S., CONSTANTZ, J., RUEHL, C. (2006). Quantifying surface water–groundwater interactions using time series analysis of streambed thermal records: Method development. *Water Resources Research* 42, 14 pp.
- HOPMANS, J.W., SIMUNEK, J., BRISTOW, K.L. (2002). Indirect estimation of soil thermal properties and water flux using heat pulse probe measurements: geometry and dispersion effects. *Water Resources Research* 38(1), 14 pp.
- INGEBRITSEN, S.E. & SANFORD, W.E. (1998). Groundwater in Geological Processes. *Cambridge University Press*, 345 pp.
- JIANG, Y. & WOODBURY, A.D. (2006). A full-Bayesian approach to the inverse problem for steady-state groundwater flow and heat transport. *Geophysical Journal International* 167, 1501–1512.
- KEERY, J., BINLEY, A., CROOK, N., SMITH, J.W.N. (2007). Temporal and spatial variability of groundwater-surface water fluxes: development and application of an analytical method using temperature time series. *Journal of Hydrology* 336(1–2), 1–16.

- KONIKOW, L.F. (2010). The Secret to Successful Solute-Transport Modeling. *Ground Water* 49, 144-159.
- LANGEVIN, C.D. & GUO, W. (2006). MODFLOW/MT3DMS- based simulation of variable density ground water flow and transport. *Ground Water* 44(3), 339–351.
- LANGEVIN, C.D., DAUSMAN, A.M., SUKOP, M.C. (2010). Solute and Heat Transport Model of the Henry and Hilleke Laboratory Experiment. *Ground Water* 48(5), 757-770.
- LANGEVIN, C.D., SHOEMAKER, W.B., GUO, W. (2003). MODFLOW-2000, the U.S. Geological Survey modular ground-water model—Documentation of the SEAWAT- 2000 Version with the variable-density flow process (VDF) and the integrated MT3DMS transport process (IMT). *U.S. Geological Survey Open-File Report* 03–426, 54 pp.
- LANGEVIN, C.D., THORNE, D.T., Jr., DAUSMAN, A.M., SUKOP, M.C., GUO, W. (2007). SEAWAT Version 4: A Computer Program for Simulation of Multi-Species Solute and Heat Transport. *U.S. Geological Survey Techniques and Methods* 6(a22), 48 pp.
- LAPHAM, W.W. (1989). Use of temperature profiles beneath streams to determine rates of vertical ground-water flow and vertical hydraulic conductivity. *Water-Supply Paper* 2337, 35 pp.
- MA, R. & ZHENG, C. (2010). Effects of Density and Viscosity in Modeling Heat as a Groundwater Tracer. *Ground Water* 48(3), 380-389.
- MARGARITA, S. (2012). Energy balance and evaporation of a bare field in the Schermer polder. Master Thesis Ecohydrology.
- MARTIN, R.J., BENDER, S.F., GAULKE, S.W., WALLACE, J. (2001). Simulation of groundwater flow and heat transport on Grand Cayman Island. *MODFLOW 2001 and Other Modeling Odysseys, Conference Proceedings*, 776–782.
- MCDONALD, M.G. & HARBAUGH, A.W. (1988). A modular three- dimensional finite-difference ground-water flow model. *Techniques of Water-Resources Investigations of the U.S. Geological Survey* 6(A1), 586 pp.
- MONTEITH, J.L. (1965) . Evaporation and environment. *Symp. Soc. Exp. Biol.* 19, 205-224

- MUNZ, M., OSWALD, S.E., SCHMIDT, C. (2011). Sand box experiments to evaluate the influence of subsurface temperature probe design on temperature based water flux calculation. *Hydrology and Earth System Sciences* 15, 3495-3510.
- NISWONGER, R.G. & PRUDIC, D.E. (2003). Modeling heat as a tracer to estimate streambed seepage and hydraulic conductivity. Heat as a Tool for Studying the Movement of Ground Water Near Streams, 81–89.
- ONDERKA, M., BANZHAF, S., SCHEYTT, T., KREIN, A. (2013). Seepage velocities derived from thermal records using wavelet analysis. *Journal of Hydrology* 479, 64-74.
- OUDE ESSINK, G.H.P. (2001). Salt water intrusion in a three-dimensional groundwater system in The Netherlands: a numerical study. *Transport in Porous Media* 43(1), 137–158.
- OUDE ESSINK, G.H.P. (2001). Saltwater Intrusion in 3d Large-Scale Aquifers: A Dutch Case. *Physical Chemical Earth* 26(4), 337-344.
- OUDE ESSINK, G.H.P., DE LOUW, P.G.B., STEVENS, S., DE VEEN, B., DE PREVO, C., MARCONI, V., GOES, B.J.M. (2009). Monitoring campaign in the occurrence of freshwater lenses in the province of Zeeland. 2007-U-R0925/A, 132pp.
- PARSONS, M.L. (1970). Groundwater thermal regime in a glacial complex. *Water Resources Research* 6(6), 1701–1720.
- POST, V.E.A. (2011). Electrical Conductivity as a Proxy for Groundwater Density in Coastal Aquifers. *Ground water* 50(5).
- PROMMER, H. & STUYFZAND, P.J. (2005). Identification of temperature-dependent water quality changes during a deep well injection experiment in a pyritic aquifer. *Environmental Science & Technology* 39, 2200–2209.
- RONAN, A.D., PRUDICK, D.E., THODAL, C.E., CONSTANTZ, J. (1998). Field study and simulation of diurnal temperature effects on infiltration and variably saturated flow beneath an ephemeral stream. *Water Resources Research* 34(9), 2137–2153.
- SILLIMAN, S.E., RAMIREZ, J., MCCABE, R.L. (1995). Quantifying downflow through creek sediments using temperature time series: One-dimensional solution incorporating measured surface temperature. *Journal of Hydrology* 167, 99–119.

- SLICHTER, C.S. (1905). Field measurements of the rate of movement of underground waters. *United States Geological Survey Water-Supply and Irrigation Paper* 140 pp.
- SMITH, L. & CHAPMAN, D.S. (1983). On the thermal effects of groundwater flow: 1. Regional scale systems. *Journal of Geophysical Research* 88(B1), 593–608.
- STALLMAN, R.W. (1965). Steady one-dimensional fluid flow in a semi-infinite porous medium with sinusoidal surface temperature. *Journal of Geophysical Research* 70(12), 2821–2827.
- STONESTROM, D.A. & BLASCH, K.W. (2003). Determining temperature and thermal properties for heat-based studies of surface-water ground-water interactions. In *Heat as a Tool for Studying the Movement of Ground Water Near Streams. USGS Circular* 1260, 73–80.
- STONESTROM, D.A. & CONSTANTZ, J. (2003). Heat as a tool for studying the movement of ground water near streams. *USGS Circular* 1260, 96 pp.
- SUZUKI, S. (1960). Percolation measurements based on heat flow through soil with special reference to paddy fields. *Journal of Geophysical Research* 65(9), 2883–2885.
- TANIGUCHI, M. (1993). Evaluation of vertical groundwater fluxes and thermal properties of aquifers based on transient temperature– depth profiles. *Water Resources Research* 29(7), 2021–2026.
- THERRIEN, R., MCLAREN, R.G., SUDICKY, E.A., PARK, Y.J. (2012). HydroGeoSphere: A Three-dimensional Numerical Model Describing Fully-integrated Subsurface and Surface Flow and Solute Transport. *Groundwater Simulations Group*, 479pp.
- THORNE, D., LANGEVIN, C.D., SUKOP, M.C. (2006). Addition of simultaneous heat and solute transport and variable fluid viscosity to SEAWAT. *Computers & Geosciences* 32, 1758-1768.
- TYLER, S.W., SELKER, J.S., HAUSNER, M.B., HATCH, C.E., TORGERSEN, T., THODAL, C.E., SCHLADOW, S.G. (2009). Environmental temperature sensing using Raman spectra DTS fiber-optic methods. *Water Resources Research* 45.
- VAN DEN EERTWEGH, G.A.P.H., NIEBER, J.L., DE LOUW, P.G.B., VAN HARDEVELD, H.A., BAKKUM, R. (2006). Impacts of drainage activities for clay soils on hydrology and solute loads to surface water. *Irrigation and drainage* 55, 235–245.

- VAN PUIJENBROEK, P.J.T.M., JANSE, J.H., KNOOP, J.M. (2004). Integrated modelling for nutrient loading and ecology of lakes in The Netherlands. *Ecological Modelling* 174 (1–2), 127–141.
- VAN REES VELLINGA, E., TOUSSAINT, C.G., WIT, K.E. (1981). Water quality and hydrology in a coastal region of The Netherlands. *Journal of Hydrology* 50, 105–127.
- VANDENBOHEDE, A. & LEBBE, L. (2002). 3D density dependent numerical model of a tracer test performed in the Belgian coastal plain. *Proceedings of the first Geologica Belgica International Meeting* 12, 223–226.
- VANDENBOHEDE, A. & LEBBE, L. (2003). Combined interpretation of pumping and tracer tests: theoretical considerations and illustration with a field test. *Journal of Hydrology* 277(1–2), 134–149.
- VANDENBOHEDE, A. & LEBBE, L. (2006). Double forced gradient tracer test: performance and interpretation of a field test using a new solute transport model. *Journal of Hydrology* 317, 155–170.
- VANDENBOHEDE, A. & LEBBE, L. (2007). Effects of tides on a sloping shore: groundwater dynamics and propagation of the tidal wave. *Hydrogeology Journal* 15, 645–658.
- VANDENBOHEDE, A. & LEBBE, L. (2010). Parameter estimation based on vertical heat transport in the surficial zone. *Hydrogeology Journal* 18, 931–943.
- VANDENBOHEDE, A. & LEBBE, L. (2010). Recharge assessment by means of vertical temperature profiles: analysis of possible influences. *Hydrological Sciences Journal* 55(5), 792–804.
- VANDENBOHEDE, A., HERMANS, T., NGUYEN, F., LEBBE, L. (2011). Shallow heat injection and storage experiment: Heat transport simulation and sensitivity analysis. *Journal of Hydrology* 409, 262–272.
- VANDENBOHEDE, A., LOUWYCK, A., LEBBE, L. (2008). Conservative Solute Versus Heat Transport in Porous Media During Push-pull Tests. *Transport in Porous Media* 76, 265–287.
- WANG, H.F. & ANDERSON, M.P. (1982). Introduction to Groundwater Modeling. Finite Difference and Finite Element Methods. Freeman, San Francisco.

WATERMARK NUMERICAL COMPUTING (2010). PEST, Model-Independent Parameter Estimation User Manual: 5th Edition. 336 pp.

WESSELING, J. (1980). Saline seepage in The Netherlands: occurrence and magnitude. *Verslagen en Mededelingen, Commissie voor Hydrologisch Onderzoek TNO* 26, 17-33.

WOODBURY, A.D. & SMITH, L. (1985). On the thermal effects of three-dimensional groundwater flow. *Journal of Geophysical Research* 90(B1), 759-767.

WOODBURY, A.D. & SMITH, L. (1988). Simultaneous inversion of hydrogeologic and thermal data, 2, Incorporation of thermal data. *Water Resources Research* 24(3), 356–372.

ZHENG, C. & WANG, P.P. (1999). MT3DMS. A modular three-dimensional multispecies transport model for simulation of advection, dispersion and chemical reactions of contaminants in groundwater systems. *Documentation and User's Guide. U.S. Army Corps of Engineers Contract Report*, 239 pp.

